Quantum-Dot Heat Engines

Josefsson, Martin

2020

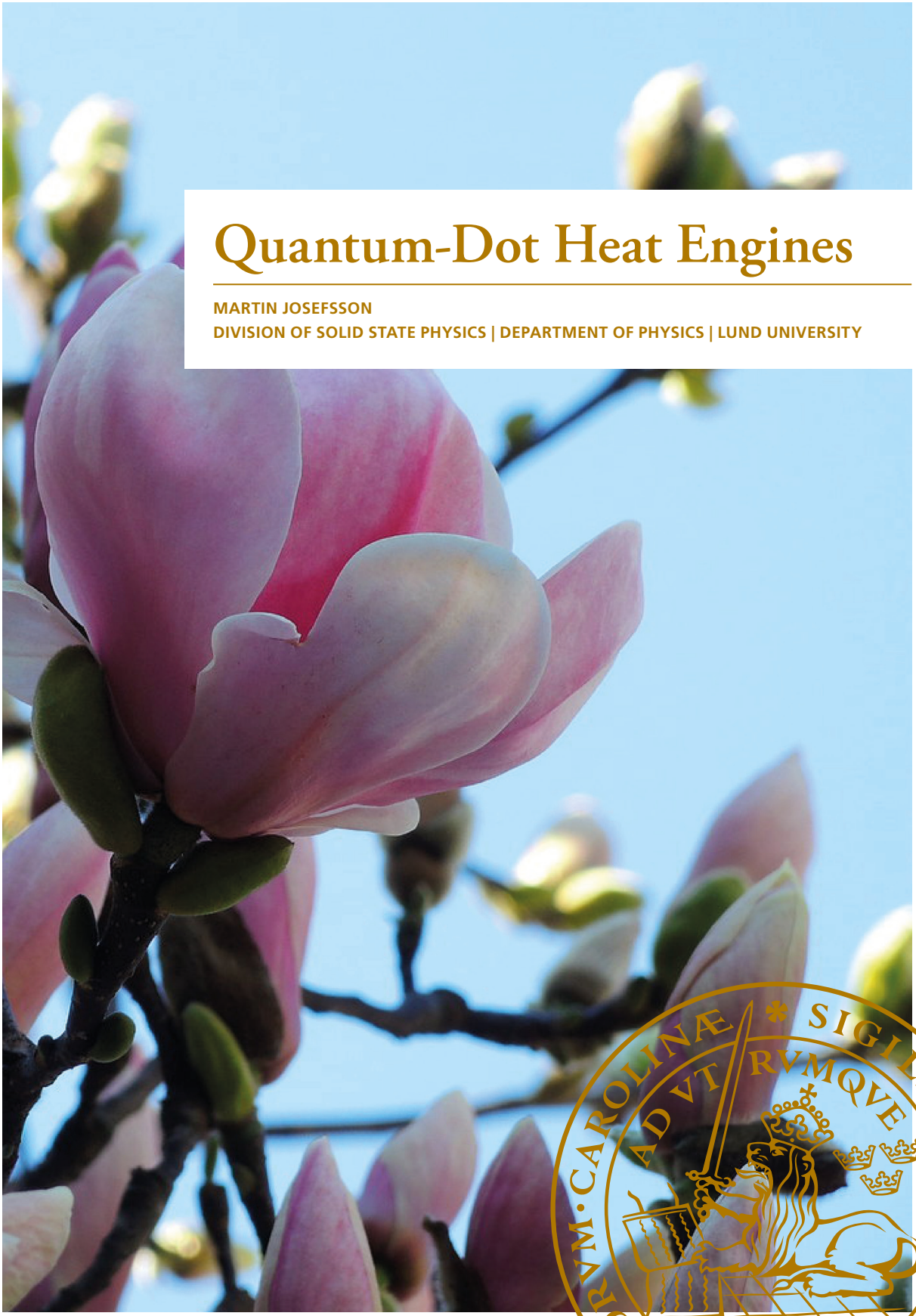

Quantum-Dot Heat Engines

MARTIN JOSEFSSON
DIVISION OF SOLID STATE PHYSICS | DEPARTMENT OF PHYSICS | LUND UNIVERSITY

Printed by Media-Tryck, Lund 2020 NORDIC SWAN ECOLABEL 3041 0903

Lund University
Faculty of Engineering
Department of Physics

ISBN 978-91-7895-496-4

Quantum-Dot Heat Engines

by Martin Josefsson

LUND
UNIVERSITY

Thesis advisor: Associate professor Martin Leijnse
Supporting advisor: Professor Andreas Wacker

DOCTORAL THESIS
which, by due permission of the Faculty of Engineering at Lund University, will be publicly defended on Wednesday, May 20th, 2020, at 9:15 in the Rydberg Lecture hall at the Department of Physics, Sölvegatan 14, Lund, Sweden.

Faculty opponent: Professor Jukka Pekola
Aalto University, Finland

Organization	Document name
LUND UNIVERSITY Department of Physics Box 118 SE–221 00 LUND Sweden	**DOCTORAL DISSERTATION** Date of disputation 2020-05-20 Sponsoring organization
Author(s) Martin Josefsson	

Title and subtitle

Quantum-Dot Heat Engines

Abstract

This thesis explores the possibilities of using quantum dots (QDs) in nanoscale energy harvesters converting heat into electrical energy, i.e. heat engines. From a theory perspective, these possibilities have been investigated for almost two decades, and interest in them seem to continuously increase over time. However, a high degree of experimental control over the manufacturing and operation of QD engines have only recently been achieved. This opens up the possibility of verifying the theory predictions and brings new questions to be answered, which is where this thesis aims at making a contribution. The author's contributions to the work that the thesis builds upon are theoretical, but are often used together with experimental results for synergistic effects.

The thesis starts with an introduction to relevant concepts in classical thermodynamics and a quantum mechanical description of electron states in QDs. This is followed by a discussion of electron transport in QDs, as well as an introduction to the master equation based approaches used to model the relevant experimental devices.

There are three studies included in the thesis, all of which have been peer-reviewed and published in scientific journals. The details of the physics relevant for each one are presented together with a summary of the studies. The first is an investigation of the performance limits of an experimental implementation of a steady-state QD heat engine, in which the Curzon-Ahlborn efficiency is observed at maximum power and the highest efficiency was in excess of 70% of the Carnot efficiency. This is the first verification that QDs can be used in high efficiency heat engines. The second study investigates how to practically optimize the output power of similar devices, and quantifies how high efficiency one can hope to reach in other implementations of QD engines. The third study proposes an experimental quantum engine based on a double QD where entangled singlet spin states are used to drive the engine. This can be viewed as entanglement acting as the engine's fuel.

Key words

quantum dot, heat engine, thermoelectric, quantum thermodynamics, quantum transport

Classification system and/or index terms (if any)

Supplementary bibliographical information	Language
	English
ISSN and key title	ISBN
	978-91-7895-496-4 (print) 978-91-7895-497-1 (pdf)
Recipient's notes	Number of pages: 146 / Price
	Security classification

Quantum-Dot Heat Engines

by Martin Josefsson

LUND
UNIVERSITY

Division of Solid State Physics
Department of Physics
Faculty of Engineering
Lund University

The front cover photo is a cropped version of a photograph by Ieva Haa licensed under CC BY 2.0.

Division of Solid State Physics
Department of Physics
Faculty of Engineering
Lund University

Box 118
SE–221 00 LUND
Sweden

ISBN: 978-91-7895-496-4 (print)
ISBN: 978-91-7895-497-1 (electronic)

Printed in Sweden by Media-Tryck, Lund University, Lund 2020

Dedicated to Ann-Mari Josefsson

Abstract

This thesis explores the possibilities of using quantum dots (QDs) in nanoscale energy harvesters converting heat into electrical energy, i.e. heat engines. From a theory perspective, these possibilities have been investigated for almost two decades, and interest in them seem to continuously increase over time. However, a high degree of experimental control over the manufacturing and operation of QD engines have only recently been achieved. This opens up the possibility of verifying the theory predictions and brings new questions to be answered, which is where this thesis aims at making a contribution. The author's contributions to the work that the thesis builds upon are theoretical, but are often used together with experimental results for synergistic effects.

The thesis starts with an introduction to relevant concepts in classical thermodynamics and a quantum mechanical description of electron states in QDs. This is followed by a discussion of electron transport in QDs, as well as an introduction to the master equation based approaches used to model the relevant experimental devices.

There are three studies included in the thesis, all of which have been peer-reviewed and published in scientific journals. The details of the physics relevant for each one are presented together with a summary of the studies. The first is an investigation of the performance limits of an experimental implementation of a steady-state QD heat engine, in which the Curzon-Ahlborn efficiency is observed at maximum power and the highest efficiency was in excess of 70% of the Carnot efficiency. This is the first verification that QDs can be used in high efficiency heat engines. The second study investigates how to practically optimize the output power of similar devices, and quantifies how high efficiency one can hope to reach in other implementations of QD engines. The third study proposes an experimental quantum engine based on a double QD where entangled singlet spin states are used to drive the engine. This can be viewed as entanglement acting as the engine's fuel.

Contents

List of publications

This thesis is based on the following publications, referred to by their Roman numerals:

I *A quantum-dot heat engine operating close to the thermodynamic efficiency limits*

M. Josefsson*, A. Svilans*, A.M. Burke, E.A. Hoffmann, S. Fahlvik, C. Thelander, M. Leijnse, & H. Linke
Nature Nanotechnology 13, p920–924 (2018)

I am one of two main authors and as such I had a leading role in writing the manuscript. All calculations were performed by me and I contributed to analyzing the experimental data as well as to guiding the experiments.

*these authors contributed equally.

II *Optimal power and efficiency of single quantum dot heat engines: theory and experiment*
M. Josefsson, A. Svilans, A.M. Burke, H. Linke & M. Leijnse
Physical Review B 99, 235432 (2019)

I had the lead role in the project where I performed the analytical and numerical calculations, contributed to analyzing the experimental data and wrote the bulk of the manuscript.

III *A double quantum-dot engine fueled by entanglement between electron spins*

M. Josefsson & M. Leijnse
Physical Review B 101, 081408(R) (2020)

As the main author and responsible for the project I performed the analytical and numerical calculations as well as wrote the majority of the manuscript.

Populärvetenskaplig sammanfattning

Denna avhandling behandlar hur vi med hjälp av nanoteknik kan direkomvandla värmeenergi till elektrisk energi. Mer specifikt hur detta kan göras genom att använda sig av komponenter som baseras på kvantprickar. En kvantprick, även kallad en artificiell atom, är en struktur eller materialbit som är så liten att elektroner som befinner sig inuti kvantpricken inte kan röra sig fritt i någon riktning. När elektroner stängs inne i så små strukturer (en typisk storlek är några tusen atomer) blir deras energi begränsad till vissa kvantiserade energinivåer, precis som för elektroner som är bundna till den positivt laddade kärnan i atomer. Därav namnet artificiella atomer. Det är denna energistruktur som gör kvantprickar intressanta när det kommer till att studera energiomvandling på nanoskalan.

Det absolut vanligaste sättet att omvandla värmeenergi till elektrisk energi är att använda värmen till att värma upp en vätska eller gas som i sin tur driver en turbin kopplad till en generator. Det är t.ex. så vi tar till vara på värmeenergin som frisläpps när vi eldar kol och gas i fossila kraftverk eller klyver atomer i kärnkraftverk. Detta tillvägagångssätt lämpar sig för storskaliga kraftverk men är inte kompatibelt med mikroskopiska och nanoskopiska komponenter. Därför studeras här istället två typer av direkomvandlande komponenter som båda baseras på kvantprickar. Syftet med forskningen som avhandlingen bygger på är främst att studera fundamentala aspekter av energiomvandling på dessa längdskalor, inte att designa kommersiellt gångbara komponenter.

Den första komponenttyp som studeras är en så kallad termoelektrisk generator i vilken en temperaturskillnad över ett material inducerar en elektrisk ström. Detta kräver att elektroner med olika energier transporteras olika bra i materialet, d.v.s. att materialet fungerar som ett energifilter. Här är kvantprickar intressanta då elektroner som transporteras genom dem endast kan ha vissa kvantiserade energier, vilket är väldigt fördelaktigt för en termoelektrisk komponent. Det har förutspåtts att en termoelektrisk generator baserad på en enda kvantprick kan ha en väldigt hög verkningsgrad, och i extrema fall till och med nå den absolut högsta verkningsgrad som tillåts enligt termodynamikens lagar. Denna förutsägelse testas i en studie som är inkluderad i avhandlingen. I den lyckades vi med

avancerad teori och experiment utförda nära den absoluta nollpunkten (-273.15 °C) verifiera att sådana komponenter faktiskt kan närma sig de fundamentala gränserna för hur effektiv energiomvandling kan vara. Samma komponent analyserades i mer detalj i en annan studie där det undersöktes vilka arbetsförhållande som krävs för att maximera komponentens elektriska uteffekt samt verkningsgrad. Resultatet av studien kan ses som tydliga riktlinjer för hur prestandan hos liknande komponenter enkelt kan optimeras.

Den andra typen av komponent som analyserats består av två sammankopplade kvantprickar där elektronerna kan hoppa mellan dem via så kallad tunnling. Speciellt för detta system är att elektronerna kan befinna sig i ett visst sammanflätat kvanttillstånd. Genom att ändra tunnelkopplingen mellan kvantprickarna går det att ändra energin hos detta tillstånd. Denna princip används för att föreslå ett experiment där en dubbekvantprick med två elektroner används för att utvinna värmeenergi från omgivningen. I förslaget börjar elektronerna i ett sammanflätat tillstånd och kopplingen mellan kvantprickarna är avstängd. I nästa steg ökas tunnelkopplingen snabbt till ett förutbestämt värde och elektronernas energiminskning tolkas som utvunnet arbete. Efter ett tag kommer värmeenergi från omgivningen att ha absorberas vilket gör att elektronerna övergått till andra energitillstånd. Till slut stängs tunnelkopplingen av igen. Efteråt befinner sig elektronerna i ett tillstånd som är nästan identiskt med det tillstånd de började i, fast utan sammanflätning. Detta är alltså ett förslag på hur vi med hjälp av kvantprickar kan använda kvantmekanisk sammanflätning för att utvinna värmeenergi. Analysen som utförts är helt teoretiskt, men med den teknik vi har idag kan det vara fullt möjligt att utföra det föreslagna experimentet inom en snart framtid.

Introduction

The topic of this thesis is energy conversion at the nanoscale. More precisely how thermal energy (heat) can be converted into another more useful form of energy, electrical energy. This subject has its roots in two of the historically most important disciplines of physics, both in regards of fundamental science and for enabling the rapid technological development of our society, namely thermodynamics and quantum mechanics. Thermodynamics is the study of energy, work and heat. It plays an immensely important role in all of the natural sciences and did allow us to understand how to best use the heat produced by burning fuel to make large machines move. In other words, how to build heat-engines, such as the steam engine, which kick-started the industrial revolution. Quantum mechanics on the other hand is used to describe tiny worlds that are far too small to be seen by the naked eye. For example, it helps us understand elementary particles, atoms, molecules and how they interact with one another. It was breakthroughs in quantum mechanics that allowed us to understand the electronic properties of materials, such as why certain materials are good conductors, and how to modify these properties to our liking. This led to the creation of the first transistor half a century ago that paved the way for the digital revolution we have experienced since. Because thermodynamics and quantum mechanics have typically been deployed to describe systems of vastly different sizes, there has historically been little interest in studying the union of the two. However, in recent years the ability manufacture materials and components with nanometer, or even atomic, precision sparked an interest in the field. Much effort has been put into answering questions such as how work, heat and entropy should be defined and understood in the quantum realm. And more importantly for this thesis, if we can create tiny heat-engines that make use of the special properties of nanoscale and quantum systems to perform as good, or even better, as their classical counterparts.

There is a myriad of different ways to create nanoscopic heat-engines where the laws of quantum mechanics become important (however, to this date very few have been demonstrated in practice), but focus here will be on engines whose central part consists of one or more quantum dots (QDs). A QD is a spatial region inside a material where electrons are in some way confined (or trapped). They are often described as artificial atoms since the electrons trapped inside them have discrete energies, just like in the orbitals of atoms.

In the research introduced in later chapters the QDs are either used in a steady state single-electron transistor setup where energy is harvested using the thermoelectric effect, or the spin dynamics of electrons on a double QD is used to extract thermal energy from its environment. However, before these engines are discussed any further this chapter attempts to provide the reader with enough background information to understand how these engines work. This is done by briefly introducing selected parts of the relevant fields of physics that the current research builds upon, and use simple, but robust, theoretical arguments to break down any underlying physical mechanism. The thesis is written with the aim that a fictitious reader with experience in physics will be able to understand most concepts and grasp the novelty of the research. It is my hope that all parts of the thesis can be read somewhat independently and I will try to emphasize the main messages so that also non-physicists can appreciate the findings, and hopefully learn something new.

The thesis is organized as follows. The first chapter introduces the scientific background needed to fully understand the main results in later chapters. It focuses on the most important concepts of classical thermodynamics and of electron states in nanoscale systems. It is written with the intent that a reader familiar with the former, but not the latter, will be able to appreciate the main results as much as a reader with the inverse experience. This is followed by a chapter describing electron transport though QD-based devices. Much emphasis is put on the theoretical approaches used to model and analyze the engines studied. That chapter is rather technical and requires a fair amount of knowledge about quantum mechanics, in particular second quantization and density matrices, to fully grasp. However, knowledge of the specific theory it is not completely necessary when going in to the remaining chapters. The topic of the third chapter is the thermoelectric effects in general, and in QD devices in particular. This is also the topic of paper I and II, which are summarized here. Moving on to chapter four, single bath (quantum) heat engines will be discussed together with the summary of paper III. Finally, the thesis ends with an outlook.

1 Classical thermodynamics

Thermodynamics is a true giant of modern science that is frequently employed in all of the natural sciences. Nowadays it is probably most associated with the descriptions of states of matter, and changes between states of matter (phase transitions), but the field is far richer than that. Here we are more interested in using it to study conversion between different types of energy. Primarily how we can take heat, which is generally considered a useless form of energy, and convert it into useful work, in our case electrical energy. This approach has great historical value as much of the foundation of what we today call thermodynamics was developed in the 18th and 19th century in order to create more efficient steam engines. These engines became widely used in the 1700s, and along with their success grew a desire to understand how to best convert heat into motion. One of the biggest breakthroughs came

with Sadi Carnot's book *Reflections on the Motive Power of Fire* [1], in which he discussed energy, power and efficiency of heat engines, as well as introduced the notion that their fundamental performance limits are independent of engine designs. Although Carnot did not include any mathematical proofs to support his claims he successfully inferred what properties a heat engine should have to maximize its performance (work and efficiency). He also argued that the maximum possible efficiency is only determined by the operating temperatures (of the heat source and heat sink, see Section 1.2), but did not calculate how high this efficiency is. Building upon this work Clausius introduced the notion of entropy [2], which is a quantity that only depends on the state of a given system. Entropy is commonly viewed as the degree of disorder of a system, but it can be more practical to think of it as a measure of a system's resistance to change. Today the concept of entropy is as central to thermodynamics as energy and work. By the late 1800s a new approach to thermodynamics, statistical mechanics, arose with contributions from many well-known physicists such as Boltzmann, Gibbs, Maxwell and Einstein [3, 4]. Statistical mechanics can be viewed as a microscopic approach to thermodynamics where properties of a system are calculated by considering collections of a great number of individual particles and their interactions. As an example, the pressure and temperature of a gas can be obtained by considering only the positions and velocities of the individual particles that make up the gas. Statistical mechanics came out as a very successful theory and is a crucial tool to have in one's toolbox when studying the thermodynamics of nanoscale systems, especially since the number of particles under consideration is typically very small. The concepts introduced in this chapter take advantage of this approach. The history of thermodynamics is of course far richer than highlighted here, but for our purposes the preceding history lesson will suffice, and we will move on to an introduction of the relevant concepts for building nanoscale heat engines.

1.1 The laws of thermodynamics

In this thesis a system is thought of as a spatial region that can accommodate particles of a certain kind, e.g. a QD that can be populated with up to a few electrons, or metallic leads (contacts) where the number of electrons become macroscopic. A system can be in one of many well-defined states where the likeliness of the system being in a particular state can be calculated using statistical mechanics. The systems under consideration are generally connected to other systems with whom they can exchange particles and/or energy. The change of a system's internal energy U is expressed as

$$dU = dW + dQ, \tag{1}$$

where the notions of work W and heat Q are introduced. This is known as the first law of thermodynamics, and will serve as a definition of heat where it makes up the part of an energy change that cannot be used to perform work, at least not directly.

The second law of thermodynamics can be expressed in several ways, but the most common interpretation is that the entropy S of an isolated system never decreases over time, i.e. spontaneous processes are always, on average, associated with an increase in entropy

$$S_{\text{final}} \geq S_{\text{initial}} \text{ or } dS \geq 0. \tag{2}$$

Equality is only found when the initial and finial states are connected by adiabatic (no heat exchange) reversible processes. A reversible process is a process without losses such that when done in reverse, by infinitesimal changes is some control parameter, is the exact inverse of the original process. This requires that the process is quasistatic, meaning that the system will remain in equilibrium at all times. A further characteristic of reversible processes is that $dS_{rev} = \frac{dQ}{T}$, for which the first law can be rewritten

$$dU = dW + TdS. \tag{3}$$

All natural processes, however, have some degree of irreversibility associated with them since almost all systems have some inherent losses, and a process is never truly quasistatic as that would require an infinite amount of time. For irreversible processes $dS_{irr} > \frac{dQ}{T}$.

A consequence of the second law is that heat always flows from a hot to a cold heat bath (also known as reservoir) in contact with one another if no energy is being spent to prevent it, or to make it move in the opposite direction. This can be understood from a simple example. Consider two reservoirs, one cold at temperature T_C and one hot at T_H, in contact with one another such that energy can be transferred between the two. If no work is being performed on, or extracted from, the system then $dW = 0$, both in total and for each reservoir. The first law provides the energy change in the hot reservoir $dU_H = dQ_H$, which must be compensated for by the change in the cold reservoir, $dQ_C = -dQ_H$, if no energy exchange with the environment is allowed. The second law states that $dS_{\text{tot}} = dS_C + dS_H \geq 0$, from which one obtains

$$dS_C + dS_H = \left(\frac{dQ_C}{T_C} + \frac{dQ_H}{T_H}\right) = \left(\frac{1}{T_C} - \frac{1}{T_H}\right) dQ_C \geq 0. \tag{4}$$

As a result, we can see that $dQ_C > 0$, i.e. the energy of the cold reservoir increases and thus heat must flow from hot to cold. One can also see that $dS_{\text{tot}} = 0$ requires either $dQ_C = dQ_H = 0$ (uncoupled reservoirs) or $T_C = T_H$ (equilibrium).

1.2 Heat engines

A heat engine uses the energy flow between reservoirs at different temperatures to generate useful work. The term heat engine has traditionally been used for devices that transform

thermal energy into useful mechanical energy, although in this thesis it will also be used to describe devices that transform thermal energy into electrical energy. A very crude diagram showing the different parts of a traditional heat engine can be seen in Fig. 1. It consists of two reservoirs, each in a thermal equilibrium state, but at different temperatures, and the central "engine" part that generates the mechanical work. The engine works by, in each cycle, absorbing heat Q_H from the hot reservoir, convert some of that thermal energy into useful mechanical energy W_{out} in its central part before depositing the remaining energy Q_C in the cold reservoir, which acts as a heat sink (as heat naturally flows from hot to cold). The second law forbids heat engines from continuously converting all thermal energy to work, and as a result also forbids them from working with only one reservoir. If the entirety of the absorbed heat in a reversible engine was converted to work then $Q_{\text{reservoir}} = T\Delta S = W_{\text{out}} < 0$, in violation of the second law since $\Delta S < 0$. The cold reservoir thus acts as a heat, and entropy, sink ensuring that $\Delta S_{\text{tot}} = \frac{Q_C}{T_C} + \frac{Q_H}{T_H} \geq 0$.

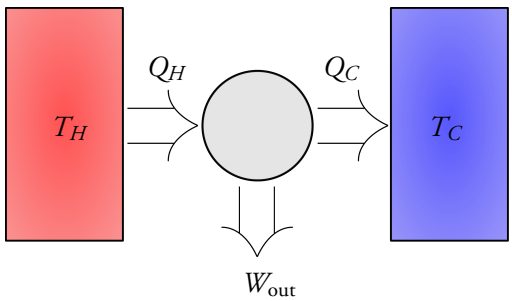

Figure 1: A crude schematic showing the components common for all heat engines: a hot reservoir at temperature T_H, a cold reservoir at temperature T_C and the central part that generates the output work (gray). The central part converts some of the heat leaving the hot reservoir Q_H into useful work W_{out} and deposits the remaining heat Q_C in the cold reservoir.

The efficiency of a heat engine is given by the ratio of the output work and the thermal energy absorbed from the hot reservoir

$$\eta = \frac{W_{\text{out}}}{Q_H}. \tag{5}$$

Carnot realized that a heat engine would generate a maximal amount of work per cycle, and be maximally efficient, only if operated reversibly [1]. In that case $\Delta S_{\text{tot}} = \Delta S_H + \Delta S_C = 0$ yielding

$$\frac{Q_H}{T_H} = -\frac{Q_C}{T_C}. \tag{6}$$

The generated work can then be obtained from energy conservation alone $W_{\text{out}} = Q_H + Q_C$, and the efficiency of a reversible heat engine is

$$\eta_C = \frac{Q_H + Q_C}{Q_H} = 1 + \frac{Q_C}{Q_H} = 1 - \frac{T_C}{T_H}. \tag{7}$$

This is known as the Carnot efficiency and is the fundamentally highest efficiency any heat engine can reach. However, η_C is derived for reversible conditions and is thus, unfortunately, accompanied with infinitely slow operation and vanishing output power. This makes it very cumbersome to experimentally verify it in a laboratory. It is nevertheless an interesting bound from a fundamental physics perspective, and it serves as a good measure of engine performance since engines that could reach η_C in the long-time limit tend to have a high efficiency also for shorter cycles. It is worth noting that there are recent claims that η_C can under certain circumstances be approach even at a finite output power, see e.g. Refs 5–7.

From a practical point of view, it is usually more important to have a high output power and a high efficiency at this power. For this reason, the efficiency at maximum power is another important performance measure. If one analyzes a heat engine whose components are ideal, where all losses in its cycle are due to finite time operation, one finds that the efficiency at maximum power can be written

$$\eta_{CA} = 1 - \sqrt{\frac{T_C}{T_H}}, \tag{8}$$

as long as the heat flow is proportional to the temperature difference [8], which is the case for most engines. This efficiency was first derived independently by Novikov [9] and Chambada [10], but became a widely known result first after the work by Curzon and Ahlborn [11]. In this thesis it will be referred to as the Curzon-Ahlborn efficiency, as is commonly done in literature. The efficiency at maximum power becomes modified for engines that couple asymmetrically to its reservoirs [12], or if the heat flux does not depend linearly on the temperature difference [13, 14], although the deviations from Eq. 8 usually remain small. Today, many well-optimized heat engines such as large power plants operate at an efficiency that lies within a few percent of the Curzon-Ahlborn efficiency [12].

1.3 Equilibrium distributions

A central concept in thermodynamics is that of equilibrium. Equilibrium states are long-time stable states that perturbed systems return to when left to relax of their own accord. In equilibrium all energy and matter flows vanish, and equilibrium states thus remain constant over time. The entropy of a system in equilibrium always takes its maximal value, which is a further characteristic of such a state. If a system is connected to an environment (a larger system) it is said to be in equilibrium with the environment when all flows between them have vanished, which requires the two systems to have the same temperature. However, the concept of temperature is not always well-defined in small isolated systems since it is a

collective property of a large number of particles,[1] and we will thus refrain from discussing temperatures in small systems. Explicit expressions for equilibrium states for different systems, derived from microscopic principles, is a central result of statistical mechanics. Below follows a short discussion of the most common such states, which are also the ones relevant for this thesis. More in-depth discussions and derivations of the results presented here can be found in all introductory text books on statistical mechanics, e.g. Ref. 4.

When a system with relatively few (micro)states is coupled to an environment at thermal equilibrium such that only energy can be exchanged, the probability of finding the system in a certain state i in equilibrium is given by the Boltzmann distribution

$$p_i = \frac{e^{-E_i/k_B T}}{Z}. \tag{9}$$

Here E_i is the energy of state i, k_B Boltzmann's constant and Z the partition function accounting for probability normalization, $Z = \sum_j^N e^{-E_j/k_B T}$, where the sum runs over all possible states. If one knows the probability distribution of a given system, be it in equilibrium or not, obtaining the entropy is a straight forward task as it is given by

$$S = -k_B \sum_i p_i \ln p_i. \tag{10}$$

When a system instead contains a macroscopic number of particles (this is referred to as a reservoir or bath) its equilibrium state can characterized by only two thermodynamic quantities: a temperature T and a chemical potential μ. μ is the energy required to add a new particle to the reservoir and is only defined for the grand canonical ensemble. If the particles in a reservoir are non-interacting fermions (e.g. electrons), such that the Pauli principle must be taken into account, its state in thermal equilibrium is characterized by the Fermi-Dirac distribution

$$f_f(\varepsilon) = \frac{1}{e^{(\varepsilon-\mu)/k_B T} + 1}, \tag{11}$$

which describes the occupation probability of a single-particle state at energy ε. When the reservoir is filled with bosons (e.g. phonons or photons) the equilibrium state is given by the Bose-Einstein distribution

$$f_b(\varepsilon) = \frac{1}{e^{(\varepsilon-\mu)/k_B T} - 1}. \tag{12}$$

[1] An effective temperature of a small system out of equilibrium can be defined when it is weakly coupled to a larger, but finite sized, reservoir with which it can exchange energy and particles. The effective chemical potential and temperature of the system is then defined as the reservoir's corresponding parameters when all energy and particle transfer between them vanish [15, 16].

1.4 Maxwell's demon and information

The validity of the second law has been challenged plenty of times. Most notable is the thought experiment by Maxwell [17], nowadays known as Maxwell's demon, that led to the discovery of the connection between thermodynamics and information. It is formulated as follows. Maxwell envisioned a box with two compartments, both of which are filled with a gas in thermal equilibrium. A gas consists of molecules, or particles, that move stochastically with random velocities, but their mean velocity is set by the temperature of the gas. Next, Maxwell considered a hatch in the wall connecting the two compartments. The hatch can move without friction such that there is no work cost associated with opening and closing it. If a fictitious being (the demon) with the ability to track individual molecules is set to operate the hatch it could, for example, open the hatch for slow particles approaching from the left and for fast particles approaching from the right. This would, after a while, result in the left compartment containing only particles with a velocity larger than the average and the right only containing slower particles. As a result, the gas in the left compartment has a higher temperature than that in the right compartment. The energy difference between two reservoirs kept at different temperatures can then be used to induce a heat flow and extract work, as discussed in section 1.2. Energy can then be extracted "for free" and the demon violates the second law as the total entropy of the system decreases without work being spent (since the hatch is frictionless). Maxwell did not reach a satisfactory explanation of how this could be the case.

The most important step towards solving this conundrum was provided by Szilard in his study of what is now known as the Szilard engine [18]. The operation of this engine is illustrated in Fig. 2. It is a minimal version of Maxwell's original demon where the box is filled with an ideal gas that consists of a single particle. The first step in the engine's cycle is to observe if the particle is in the left or right half of the box. Once this information is acquired a partition is inserted (without friction) in the middle of the box, and a weight is connected to the partition. Then, by letting the box exchange energy with an environment at temperature T it is possible to lift the weight by letting the gas expand. If the expansion is isothermal (T of the gas is kept constant), i.e. reversible, the total work performed by the ideal gas on the weight is

$$W = \int dW = \int_{\frac{V_{\text{box}}}{2}}^{V_{\text{box}}} P dV = \int_{\frac{V_{\text{box}}}{2}}^{V_{\text{box}}} \frac{k_B T}{V} dV = k_B T \ln 2. \tag{13}$$

After the expansion is completed the weight is disconnected and the partition removed, leaving the system in its initial state and a new cycle can begin. Thus, in each cycle $k_B T \ln 2$ of heat is converted into work, decreasing the entropy of the environment by $k_B \ln 2$. However, $\Delta S_{\text{gas}} = 0$ since the particle has the same initial and final state, which yields $\Delta S_{\text{total}} < 0$ in violation of the second law. Szilard argued that the decrease of the reservoir's entropy must be compensated for by an increase in entropy in some other part of the

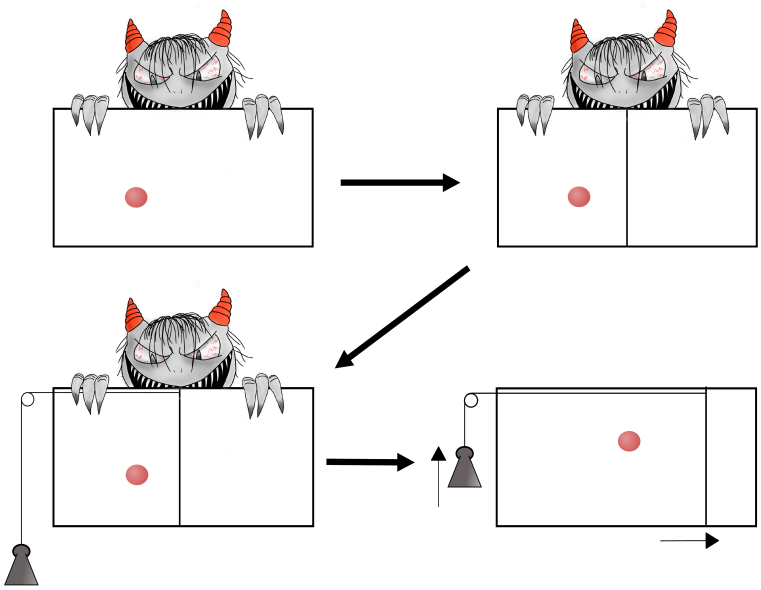

Figure 2: Schematic of the Szilard engine. Top left - the demon observes where the particle is located. Top right - the demon insert a partition (frictionless). Bottom left - the demon attaches a weight to the partition. Bottom right - The gas gets to expands isothermally. The resulting work lifts the weight.

system. Two decades later Brillouin theorized that it is measurements, i.e. acquisition of information, that leads to an entropy increase [19], which was the first, and very important, link between thermodynamics and information. According to that theory acquiring a single bit of information (in this case: is particle to the left or right, which is equivalent to 0 or 1) is associated with an entropy increase of at least $k_B \ln 2$, and thus also energy dissipation $Q \geq k_B T \ln 2$. Independently, Landauer investigated the minimum energy cost associated with memory erasure in a computer, and formulated what we now know as Landauer's bound, that the minimum energy cost for *erasing* a bit of information is $k_B T \ln 2$ [20]. This is the fundamental energetic limit of computing. The final piece in the puzzle was provided by Bennett who made the connection between Maxwell's demon and Landauer's bound. Furthermore, he showed that the measurements (and in fact any computation) can be performed reversibly, without an energy cost [21, 22]. In the Szilard engine this means that in order to start a new cycle one must erase the demon's memory from the previous cycle, which costs energy and thus no net work is extracted. Alternatively, arguing from an entropy point of view, the entropy decrease of the bath is exactly compensated for by the entropy increase of the memory (where the demon stores the information from measuring the particle's position) and the total entropy change in one cycle is $\Delta S_{\text{tot}} = 0$. The second law will thus not be violated.

2 Nanoscale systems

The development of the theory of quantum mechanics in the early 20th century provided us with the tools to study and understand the mesoscopic and nanoscopic worlds that are too small to be observed with the human eye, even with the most advanced optical microscope. The theory was during its first decades only used to describe natural systems such as atoms, molecules and crystalline materials. But if we fast forward to today, technological advancements have made it possible to manufacture artificial systems small enough for a classical description to fail, and a quantum mechanical description to be necessary also here. The remainder of this chapter is devoted to a quantum mechanical discussion of how electrons behave inside nanoscale systems, and how different kinds of such systems can be created.

2.1 The wave function

In quantum mechanics all matter is treated as waves, which is in stark contrast to classical physics where a particle's state can be assigned a well-defined position and velocity. Information of the classical state combined with knowledge of the particle's surrounding environment, as well as its intrinsic properties such as charge and mass, is enough to deterministically predict the particle's time evolution and the outcome of any measurement. In a wave description of matter the state information is instead encoded in the wave function of the particle, and the wave function's time evolution can be calculated deterministically. However, the outcome of measurements on the particle are inherently stochastic. The idea that all particles, as well as all physical objects, can be viewed as waves was introduced by Louis the Broglie in 1924 [23]. He proposed that an object with mass m is associated with a wavelength $\lambda_{dB} = \frac{h}{mv}$, where h is Planck's constant and v the objects velocity. As far as we know this description remains valid for all particles, but for macroscopic objects such as a human being or a football λ_{dB} is too small for the wave description to be meaningful, and it is only used for very light particles such as elementary particles, atoms and molecules.

de Broglie's ideas led to Erwin Schrödinger gaining enough insight to write down the general equation governing the dynamics of any quantum mechanical wave function $|\Psi(t)\rangle$ [24],

$$i\hbar\frac{\partial}{\partial t}|\Psi(t)\rangle = H|\Psi(t)\rangle. \tag{14}$$

(the reader is assumed to be familiar with the Dirac notation, otherwise see e.g. Ref. 25). Here $h = 2\pi\hbar$ and H is the Hamilton operator, which incorporates all terms corresponding to the kinetic and potential energy of the system. When the Hamilton operator is time-

independent and relativistic effects are neglected Eq. 14 can be rewritten as

$$\left(\frac{-\hbar^2}{2m}\nabla^2 + V(\mathbf{r})\right)\psi(\mathbf{r}) = E\psi(\mathbf{r}), \tag{15}$$

where $\Psi(\mathbf{r}) = \langle \mathbf{r}|\Psi\rangle$ is the particle's position-space wave function, E its total energy and $V(\mathbf{r})$ describes the potential landscape the particle experiences. $|\Psi(\mathbf{r})|^2$ is interpreted as the probability distribution for finding the particle at position $\mathbf{r}$ in a measurement.

The complexity of solving Eq. 15 depends on $V(\mathbf{r})$, and for most physical systems no analytical solution exists. However, for later discussions it is illustrative to look at two cases where the solutions are particularly simple. First, the solutions to Eq. 15 for a free electron ($V(\mathbf{r}) = 0$) are plane waves $\psi(\mathbf{r}) \propto e^{-i\mathbf{q}\cdot\mathbf{r}}$ with wave vector $\mathbf{q}$. The particle's energy is given by $E = \frac{\mathbf{p}^2}{2m}$ where $\mathbf{p} = \hbar\mathbf{q}$ denotes the momentum. If an electron is instead trapped in a cube with infinitely high potential walls ($V(\mathbf{r}) = \infty$ outside the cube) and side-length L, its position-space wave function is $\psi(\mathbf{r}) \propto \prod_{r=x,y,z} \sin\frac{n_r\pi r}{L}$, $n_r = 1, 2, 3...$ In this case the wave vector only takes discrete values $k_r = \pi n_r L^{-1}$, and the energy is $E = \frac{\hbar^2\pi^2}{2mL^2}(n_x^2 + n_y^2 + n_z^2)$. The take away message from this is that the energy of free electrons can take any (positive) value as $\mathbf{q}$ will be a continuous variable, whereas the energy for trapped electrons is limited to discrete values.

2.2 Electrons in solids

Obtaining a full quantum mechanical description of solid materials is an extremely hard problem due to the presence of an astronomical number of positively charged nuclei, as well as negatively charged electrons, who all interact with one another electrostatically. An exact treatment would require finding the *many body wave function* of all particles in the solid, a hopelessly complex task. Realizing that the kinetic energy of the nuclei is much lower than that of electrons (due to the larger nuclear mass) allows for treating the electrons and nuclei separately. However, even with this simplification the task of finding the *many electron wave function* is an incredibly hard problem, and great effort is being put into accurately calculating the electronic structure of solid materials using several sophisticated techniques [26]. Here we will not concern ourselves with those techniques, but instead use fairly simple theoretical arguments to deduce how electrons behave inside solid materials, leading up to how they behave in nanostructures. Such a simplified approach sacrifices detailed information in exchange for clarity.

Our starting point will be to consider electrons inside ideal crystalline materials where all atoms are perfectly ordered in repeating patterns in all spatial directions. In this case the potential due to the ordered nuclei, $V_{\text{per}}(\mathbf{r})$, is a perfectly periodic function in real space, i.e. $V_{\text{per}}(\mathbf{r}) = V_{\text{per}}(\mathbf{r} + \mathbf{a})$ where $\mathbf{a}$ is a lattice vector connecting two repeating unit cells

in an arbitrary direction. The shape of this potential is rather complex as the potential an electron experiences due to a single nucleus with atomic number Z_N at position $\mathbf{r_p}$ is given by the Coulomb interaction between the charges

$$V_C(\mathbf{r}) \propto \frac{-e^2 Z_N}{|\mathbf{r} - \mathbf{r_p}|}. \tag{16}$$

The total potential from the lattice is a sum of the Coulomb potentials for all nuclei at different $\mathbf{r_p}$. If one assumes that it is possible to treat the problem as an effective one-particle problem, e.g. by incorporating the effects of all other electrons as a mean field [27], the problem is reduced to finding the solution to the Schrödinger equation with a periodic potential. With these assumptions Bloch's theorem states that the energy eigenfunctions, i.e. solution to Eq. 15, can always be expressed as [28]

$$\Psi_{\mathbf{k}}(\mathbf{r}) = u_{\mathbf{k}}(\mathbf{r}) e^{i\mathbf{k}\cdot\mathbf{r}}, \tag{17}$$

where $u_{\mathbf{k}}(\mathbf{r})$ is a function with the same periodicity as the potential.[2] A possible one-dimensional Bloch wave $\Psi_{k_x}(x)$ is illustrated in Fig. 3.a. A special property of the Bloch waves is that they are invariant under a shift of a reciprocal lattice vector $\mathbf{G} = \mathbf{a}^{-1}$, i.e. $\Psi_{\mathbf{k}}(\mathbf{r}) = \Psi_{\mathbf{k}+\mathbf{G}}(\mathbf{r})$, or by multiples of a reciprocal vector. Furthermore, the energy dispersion follows the same periodicity $E(\mathbf{k}) = E(\mathbf{k} + \mathbf{G})$. It is thus sufficient to restrict any analysis to $|\mathbf{k}|$-values lesser than a single reciprocal lattice vector, for example $|k| \leq \pi/a$ in a one-dimensional crystal with lattice constant a. This region of $\mathbf{k}$-space is commonly referred to as the first Brillouin zone.

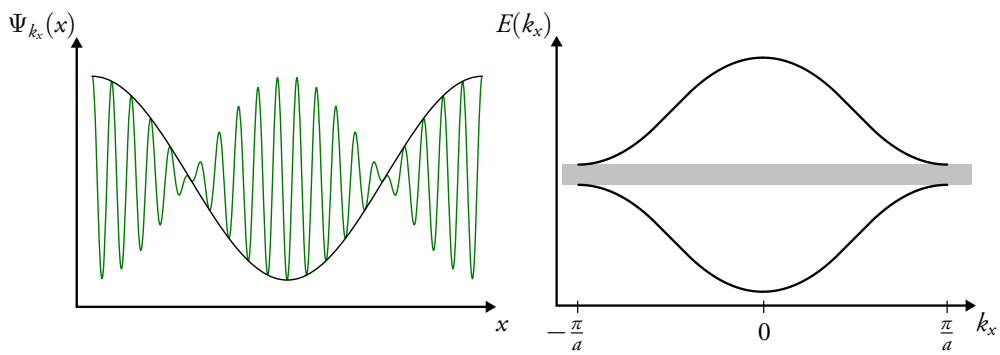

Figure 3: a) A possible one-dimensional Bloch wave function according to Eq. 17. The green line represents $u_{k_x}(x)$, which oscillates at the same frequency as the crystal lattice, and the black line is real part of e^{ikx}. b) Illustration of a one-dimensional band structure. The grey area represents an energy range with no allowed states. The continuum of allowed states is called an energy band, and the difference between bands is called a band gap. A typical bulk material will host many bands.

[2] A derivation of Bloch's theorem can be found in Chap. 7.1 of Ref. 29, in appendix C of Ref. 30, and in many other books on solid state physics.

Bloch's theorem thus provides us with some properties of the electronic wave functions in solid materials based on symmetry arguments alone, but so far we do not have any explicit expressions for neither $\Psi_{\mathbf{k}}(\mathbf{r})$ nor $E(\mathbf{k})$. Obtaining such expressions requires solving Eq. 15, usually using some approximative method, while requiring that the solutions have the aforementioned properties. This can for example be done by assuming that the periodic potential is weak and the wave functions resemble plane waves, such that the problem can be treated using second order perturbation theory with $V_{\text{per}}(\mathbf{r})$ as the perturbing potential. Another approach is to express the wave functions as sums of atomic orbitals from atoms at the different lattice sites. These, and other, approaches are discussed in e.g. Refs. 29–31 and other standard textbooks on solid state physics. The resulting energy dispersion $E(\mathbf{k})$ will be similar to the one sketched in Fig. 3.b for a one-dimensional crystal. For the sake of simplicity, the discussion will be restricted to one dimension, but extensions to higher dimensions follow the same reasoning. Close to the center of the Brillouin zone $E(\mathbf{k})$ will be (almost) parabolic, but close to the edges of the Brillouin zone there will be large deviations from the free electron case. As a result, an energy band without electron states opens up close to the zone border.

The presence of a periodic potential thus creates bands of energies for which there are no solutions to the Schrödinger equation. There will be one forbidden band for each k-value that is a multiple of $\frac{\pi}{a}$, but in Fig. 3.b the entire band structure is moved to the first Brillouin zone without loss of generality. The emergence of energy bands in solid materials and the filling of these bands allow us to understand the difference in electric properties between different materials. When filling the bands with electrons the Pauli principle must be obeyed. It states that any state characterized by a unique set of quantum numbers can only be occupied by a single electron. In solid materials this means that each state corresponding to a $\mathbf{k}$-value at a specific energy can be populated only by two electrons with opposing spins. When accounting for the electrons originating from all the individual atoms that make up the crystal the total number of electrons is enormous, and several band will be completely filled. We differentiate between metals, semiconductors and insulators based on the filling of the bands as follows. Metals have a band that is not completely filled with electrons, i.e. the chemical potential is located in a band, and it only takes a small amount of energy to excite electrons at the chemical potential to another state. As a result, when the electrons in the band experience a force, e.g. by an applied electric field, the balance between filled states with positive and negative $\mathbf{k}$ that exists in equilibrium is easily disturbed. We thus get a net $\mathbf{k}$-value in total, leading to a net crystal momentum $\tilde{\mathbf{p}} = \hbar\mathbf{k}$, and a net transport of electrons. In contrast, insulators and semiconductors have their chemical potential located in between bands and it requires a lot of energy (determined by the band gap) to excite electrons and get transport. These materials are hence poor conductors. However, semiconductors have a fairly small band gap (usually ~ 1 eV) compared to insulators, making it easier to excite electrons to the next band. Furthermore, it is possible to introduce impurities with electronic states in the band gap into semiconductors (i.e. doping). The

electrons in these states are easily excitable - thermal energy from the surroundings is often enough - which provides engineers with a means of controlling a material's conductivity, which has been absolutely crucial for the success of digital technologies.

For the remaining part of this thesis only semiconductors will be of interest. The highest occupied band in a semiconductor is called the valence band and the lowest unoccupied band the conduction band. In the experimental devices presented in a later chapter only the conduction band is relevant, and we will focus solely on that from hereon. The semiconductors in those devices are highly n-doped resulting in the chemical potential lying inside the conduction band, as opposed to the undoped case. In general, much of the interesting physics in the conduction band takes place near the band edge where $E(\mathbf{k})$ has a minimum. In Fig. 3.b this happens around $\mathbf{k} \approx 0$ and one can see that the bands are almost parabolic in this region (this is also case for band structures obtained using more sophisticated methods [31]), much like for free electrons, albeit not necessarily with the same derivative. This observation is important as it allows us to the define an effective mass of the electrons, m^*, as

$$\frac{1}{m^*} = \frac{1}{\hbar^2}\frac{\partial^2 E(\mathbf{k})}{\partial k^2}, \tag{18}$$

allowing us to treat electrons in the conduction band as free electrons with mass m^* such that their kinetic energy is $\frac{\hbar^2 k^2}{2m^*}$. Formally, the effective mass is a tensor as it will depend on the orientation it is evaluated at in reciprocal space, but for our purposes it is sufficient to consider it to be a constant parameter that is material dependent.

2.3 Effective mass approximation

Up until this point only homogeneous bulk materials have been considered when discussing how electrons behave in solids. However, when modeling nanostructures these conditions need to be relaxed. As the name implies, nanostructures are typically far from bulk materials, and they will typically consist of more than one material, i.e. they are heterostructures. In order to arrive at a description of electronic states in these structures we start by addressing how electrons behave in heterostructured materials using the effective mass approximation. In this approximation one assumes that a perturbing potential $V(\mathbf{r})$ exists in addition to the lattice periodic potential $V_{\text{per}}(\mathbf{r})$. $V(\mathbf{r})$ can e.g. describe the potential of an impurity atom used for doping, or the resulting potential landscape in heterostructured materials.

Our goal is to solve the Schrödinger equation for the total potential, $V_{\text{per}}(\mathbf{r}) + V(\mathbf{r})$, and a convenient starting point is to identify that the Bloch states describing electrons experiencing $V_{\text{per}}(\mathbf{r})$ alone form a complete basis set [28]. If these states are known it is possible to express any other wave function as a series expansion in these Bloch states. If we denote

the wave function that solves the Schrödinger equation for the total potential as $\phi(\mathbf{r})$ the expansion in Bloch states (see Eq. 17) is expressed as

$$\phi(\mathbf{r}) = \sum_n \int_{-\frac{\pi}{a}}^{\frac{\pi}{a}} \tilde{\chi}_n \Psi_{n,\mathbf{k}}(\mathbf{r}) d^3k, \tag{19}$$

where n is a band index and $\tilde{\chi}_n$ the expansion coefficients. If only states in a narrow $\mathbf{k}$-range contribute significantly to the integral, e.g. only states close to the bottom of the band, and if we assume that $u_{n,\mathbf{k}}(\mathbf{r})$ varies slowly with $\mathbf{k}$ compared to the plane wave part, it is possible to rewrite

$$\Psi_{n,\mathbf{k}}(\mathbf{r}) \approx \Psi_{n,0}(\mathbf{r}) e^{i\mathbf{k}\cdot\mathbf{r}}. \tag{20}$$

With these assumptions one can perform an inverse Fourier transform of Eq. 19 to obtain

$$\phi(\mathbf{r}) \approx \chi(\mathbf{r}) \Psi_{n,0}(\mathbf{r}). \tag{21}$$

Assuming that it is possible to exclude all bands save one from the expansion, for example if the band gap is large, one can insert the new wave function into the Schrödinger equation. After some mathematical tricks one arrives at [32–34],

$$\left[\epsilon_n(-i\nabla) + V(\mathbf{r})\right] \chi(\mathbf{r}) = E\chi(\mathbf{r}), \tag{22}$$

which is the Schrödinger equation for the so-called envelope function $\chi(\mathbf{r})$, but with an effective Hamiltonian. Here, $\epsilon_n(-i\nabla)$ is the band structure for band n expanded as a power series, in which $\mathbf{k}$ is replaced by $-i\nabla$. Close to the band edge, such that a parabolic expansion of the band is sufficient, Eq. 22 can be rewritten as

$$\left[-\frac{\hbar^2}{2m}\nabla\frac{1}{m^*(\mathbf{r})}\nabla + V(\mathbf{r})\right] \chi(\mathbf{r}) = (E - E_C)\chi(\mathbf{r}), \tag{23}$$

where E_C is the conduction band edge, and a spatial dependence of the effective mass is taken into account. This is a remarkable result as the energy of the state only depends on the envelope function, which in turn only depends on the perturbing potential and not the periodic potential of the crystal lattice. The effective mass approximation is thus very useful when studying heterostructured materials, but it is worth noting that the assumptions made in order to obtain this result are not guaranteed to be valid and must be checked for each system under consideration. However, for many relevant semiconductor structures they remain valid [35], and we will thus use the effective mass approximation and the envelope function description when discussing the electronic structures of low dimensional semiconductor systems.

The simplest possible heterostructure is the combination of two bulk materials, A and B, such that there is a sharp interface between the two at $x = 0$. Since the materials are macroscopically large in two dimensions, the y- and z-components of the wave function will

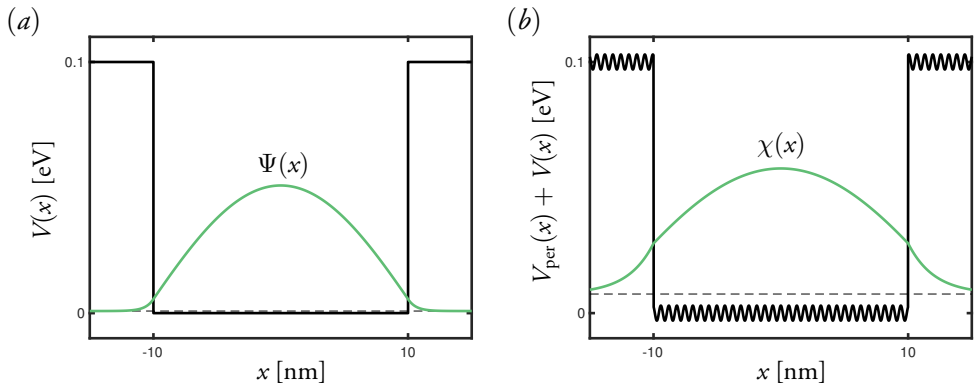

Figure 4: Comparison between the wave function and envelope function for a square potential well. a) shows a perfectly square potential well and the wave function for the ground state of an electron trapped in the well (green line). b) shows a simplification of the real potential an electron experiences when the potential well is created using a heterostructure. The envelope function (shown in green) is calculated using the effective mass $m^* = 0.067m_0$ inside the well and $m^* = 0.1m_0$ outside the well. The energy of the electron in relation to the bottom of the well is illustrated by the vertical dashed lines.

be simple plane waves, and it is enough to study the x-dependence of the envelope function. Continuity of the wave function and current conservation provides the boundary conditions

$$\chi_A(0^-) = \chi_B(0^+), \tag{24}$$

$$\frac{1}{m_A^*}\frac{d\chi_A(x)}{dx}\Big|_{x=0^-} = \frac{1}{m_B^*}\frac{d\chi_B(x)}{dx}\Big|_{x=0^+}. \tag{25}$$

The envelope function is obtained from solving Eq. 23 when imposing the boundary conditions in Eqs. 24-25.

An example of a χ in a heterostructure is shown in Fig. 4 where $V(x)$ takes the shape of a one-dimensional square potential well (y- and z-components are ignored). The solution for χ looks similar to that of the free particle trapped in a finite potential well, with only two noticeable differences: the derivative of χ is not continuous at the edge of the well due to Eq. 25, and the energy obtained using the effective mass approximation is larger due to the lower effective mass of the particle inside the material.

The take-away message from this section is that when the effective-mass approximation is valid, it is enough to know the effective mass(es) and the overall potential structure of a heterostructure or nanostructure to solve the Schrödinger equation and obtain the energy spectrum. The details of the periodic potential from the underlying crystal lattice can safely be ignored.

2.4 Density of states

Structures with length scales in the nanometer range are rich in terms of the amount of physical phenomena that can be studied using them, especially since their electronic structure becomes highly modified compared to bulk systems. A qualitative understanding of why this is the case can be obtained using the effective mass approximation introduced in the previous section. When free electrons experience a confining potential whose length scale is on the order of their de Broglie wave length, quantum confinement effects become important. The same holds true for electrons inside semiconductors (or other materials) where instead the confinement of the envelope function becomes important, as it determines an electron's energy. The exact shape of the energy spectrum of actual low dimensional structures will of course depend on the specifics of the system, but by only looking at a crude version of the confining potential one can usually get a qualitative understanding of how the electrons behave in the system. Some problems are particularly easy to analyze as the envelope function can many times be factorized into separate parts for each spatial dimension $\chi(\mathbf{r}) = \chi_x(x) \cdot \chi_y(y) \cdot \chi_z(z)$, and in turn the energy turns into a sum $E(\mathbf{k}) = E_x(k_x) + E_y(k_y) + E_z(k_z)$. Whether this is possible or not depends on the potential, its symmetries, and the choice of coordinate system, but for the structures relevant here we assume this will be the case. An example was shown in Fig. 4 where an electron experienced a 1D potential in the shape of a square quantum well, and $\chi(x)$ resembled the text book solution for the particle in a box problem. Along the remaining spatial dimensions $\chi(\mathbf{r})$ will behave like plane waves.

Structures with confining potentials in different number of dimensions will have vastly different energy spectra. This is quantified when calculating, or measuring, a system's density of states (DOS). If one assumes that the effective mass approximation is valid the energy dependence of the DOS for samples of different dimensionality is given by

$$\rho_n(E) = \theta(E - E_n) \cdot \begin{cases} \sqrt{\frac{2\pi m^*}{\hbar^2}}(E - E_n)^{-\frac{1}{2}}, & \text{1D} \\ \frac{4\pi m^*}{\hbar^2}, & \text{2D} \\ \frac{8\pi\sqrt{2}(m^*)^{\frac{3}{2}}}{\hbar^3}(E - E_n)^{\frac{1}{2}}, & \text{3D} \end{cases}, \tag{26}$$

where θ is the Heaviside step function. In Eq. 26 the index n refers to a band and E_n the band edge in 3D, whereas n refers to a so-called sub-band with energy E_n in one and two dimensions. Different sub-bands correspond to different quantum numbers for the part of the wave function that experiences quantum confinement. The DOS for systems of different dimensionality is illustrated in Fig. 5, which includes multiple sub-bands. The figure also shows the DOS for a 0D object. In that case all components of $\mathbf{k}$ are discrete, resulting in a completely discrete energy spectrum, much like for electrons bound to a nucleus in an atom. In reality, nanoscale systems rarely have a pure 2, 1, or 0D DOS, and the actual DOS will have some deviations from those sketched in Fig. 5.

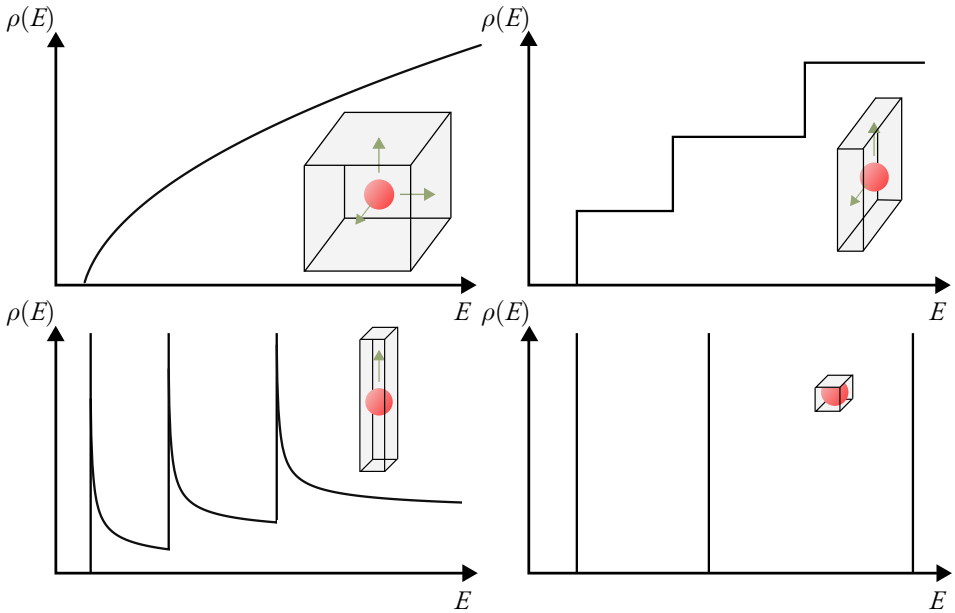

Figure 5: Density of states for systems of decreasing dimensionality, from 3D to 0D as illustrated by the insets in the figure where arrows show the dimensions along which the electrons can move freely.

2.5 Nanoscale semiconductors

The term nanoscale structure, or nanoscale semiconductor, is in this thesis used for semiconductor samples with some feature in the in the nanometer range that makes the electrons experience a confining potential in at least one dimension. Creating these structures in a lab is in itself a very complicated task, and the topic of finding new and optimized manufacturing strategies occupy entire research fields. An overview of the manufacturing of these structures is beyond the scope of this thesis and we will take their existence for granted.

Perhaps the most straight forward nanostructure is a slab of material A sandwiched in between bulk pieces of another material B, as in Fig. 6. If the conduction band edge of material A (e.g. GaAs) is lower than that of material B (e.g. AlGaAs) the low energy electrons in the conduction band of material A will experience a confining potential in the z-direction [36], at least as long as there is no overlap between the valence band in B and conduction band in A. This structure is referred to as a quantum well, and its DOS resembles that of a 2D system in Fig 5. If the sample is doped such that there is a non-negligible number of electrons in the conduction band of material A, this structure is also commonly referred to as a two-dimensional electron gas (2DEG). It is named after the simple theoretical model used to describe the electrons in the structure, in which the electrons behave as free electrons (with an effective mass) in two dimensions. In general, it is not necessary for the sample to have the same material B on both sides, as long the electrons' movement is confined to a plane, and it is sometimes more useful when one side consists

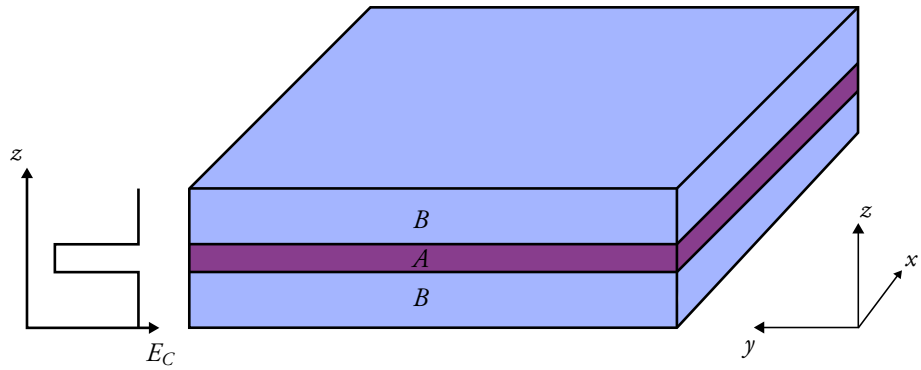

Figure 6: Quantum well sample made by sandwiching a material A with low E_C (energy of the conduction band edge), such as GaAs, between bulk pieces of a material B with a higher E_C, e.g. InGaAs. This effectively creates a quantum well in the z-direction, as illustrated in the figure, but low energy electrons in material a A are still free to move in the x- and y-directions.

of a high band gap semiconductor and one of an insulator. A 2DEG can also be created in semiconductor-insulator-metal system where a high voltage applied to the metal attracts (or repels) electrons, effectively forming a thin conductive layer close to the insulator [37]. When done in a bulk system the electrons can move freely in two dimensions.

One dimensional structures, i.e. quantum wires, can be created by either manufacturing thin wire-like segments of a semiconductor (or other material), or by further confinement of electrons in a 2DEG, see Fig 7. The former can be achieved by putting a thin segment of a semiconducting material on an insulator [38]. Alternatively, it is possible to manufacture natural wire-like structures such as carbon nanotubes [39], or so-called nanowires, which can conveniently be created by a bottom-up approach [40, 41]. For these wires the confining potentials are either oxide layers on their surfaces, the substrate they are lying on (if lying) or the vacuum/air surrounding the wire. In the second approach metallic contacts are put on top of the 2DEG (or rather on top of the insulator acting as the barrier on one side of the 2DEG) in such a fashion that an applied voltage on the contacts can restrict the electrons' movement to one dimension [42].

The most relevant structures for this thesis are, however, quantum dots (QDs). Electrons inside QDs are confined in all spatial directions and their energy spectrum will thus be discrete (see Fig. 5). Illustrations of three different kinds of QDs are shown in Fig. 8. Perhaps the conceptually most simple way to create them is to manufacture semiconducting nanoparticles where the small size of the particle accounts for the confinement of the electrons. It is also common to start from a 2DEG and use metallic contacts to create a confining potential for the electrons also in the x- and y-directions, effectively creating a 0D object [43, 44]. In the same spirit it is possible to create devices where applied electrical potentials pinch

off a nanowire, trapping electrons in a small segment of the wire [45]. The QDs used in the research for this thesis are however created using heterostructured nanowires. An example is shown in Fig. 8(b) where segments of a high band gap material (e.g. InP), separate parts of the low band gap nanowire (e.g. InAs) [46]. The conduction band edge of InAs is lower than that of InP (same principle as in Fig. 6) and any electron between the InP barriers will, in addition to the radial confinement, experience a confining potential along the wire if its energy is close to the bottom of the band. It is also possible to create QDs in homostructured nanowires where potential barriers can instead be created by changing the crystal structure of the nanowire [47, 48]. This is based on the fact that the band gap and the energy for the conduction band on-set depend on the crystal structure.

The discrete energy spectrum of QDs have made them widely used in optical applications, such as florescent marking in biological and medical applications [49, 50], or color filtering in electronic displays [51, 52]. This is because the light they emit is fairly monochromatic and its frequency is determined by the width of the confining potential, i.e. the size of the QD. In research environments QDs are often also used in electronic components, as will be the case in the remaining chapters, and as quantum bits for quantum information research [53–57].

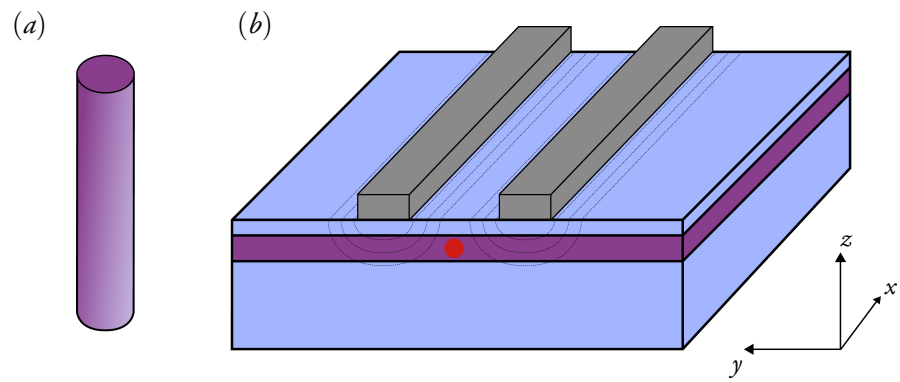

Figure 7: Example of approaches for creating quantum wires. a) Illustration of a semiconductor nanowire in which electrons are free to move along the wire, but the thin diameter restricts the wave function to small x- and y-values. b) A wire can instead be created by further confinement of electrons in a 2DEG by applying an electrical potential to contacts (gray) on top of the sample. If the additional potential from the contacts (illustrated by dashed lines) repels electrons it is possible to create an effectively 1D potential valley between the contacts. The cross section of the resulting quantum wire is illustrated by the red circle.

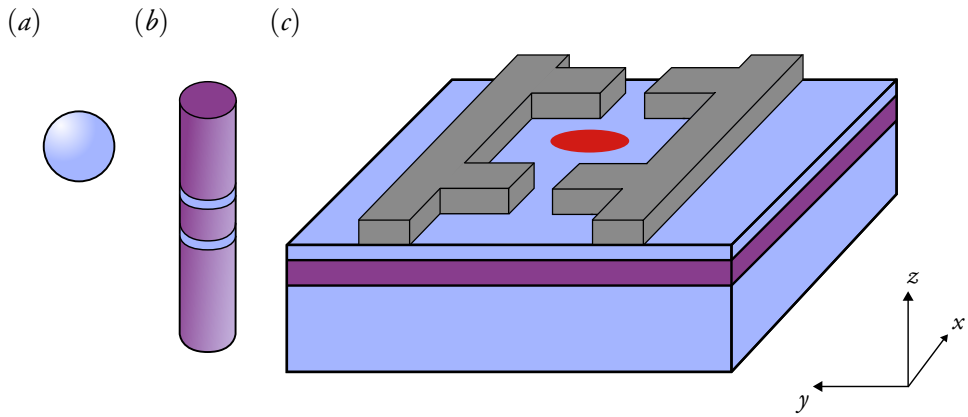

Figure 8: Three strategies for creating QDs. a) A semiconducting nanoparticle. b) Segments of a high band gap material (blue) in a low band gap nanowire (purple) can create potential barrier for electrons in the bottom of the conduction band. A QD is created between the segments of material B (defined in Fig. 6). c) Electrons in a 2DEG can be further confined by electric potentials when applying a voltage to deposited metallic contacts (gray). The red area illustrates that electrons can be trapped between the contacts if the contact geometry allows it. There are usually some openings in the contacts to allow for a tunable tunnel coupling between the QD and the rest of the 2DEG (for more info see the next chapter, which discusses transport through QDs).

Transport through quantum dots

Having motivated how electrons behave inside nanostructures we can now begin to understand transport in QD devices, and later also how to make heat engines that utilize QDs. The transport problem, i.e. accurately modeling particle and energy flows in these devices falls under the general topic of open quantum systems. Here the term open refers to the quantum system being connected to some macroscopic environment, which is what will allow us to extract work in the end. This chapter contains descriptions of the transport theories used to model the devices in the remaining chapters. It begins with an overview of electron transport in the QD-based single electron transistor, which is the experimental setup used in papers I and II. Emphasis is put on general properties and a phenomenological understanding. This is followed by a detailed description of the theory used in papers I and II to model said electron transport, the real time diagrammatic technique. The chapter ends with a short discussion of the Lindblad master equation, which was used to obtain the results in paper III.

3 Single electron transistor

A single electron transistor (SET) consists of a small object, on which electrons interact strongly, in close proximity to large metallic electron reservoirs, see Fig. 9 for a schematic. The central object can be a small metallic particle where quantization effects need not be important due to an almost continuous DOS at high energies, which is reached since metallic islands contain a large number of electrons [58]. Or, as will be the case here, it can be a semiconducting QD with discrete energy levels for electrons in the bottom of the conduction band. The QD is located close to the reservoirs so that the electron wave functions in the reservoir and the QD have a finite overlap, making it possible for electrons to tunnel between them. In addition, a third contact (referred to as gate), usually the substrate itself, is used to tune the electrical potential of the QD. The different kinds of QDs described in the previous chapter can all be used in a SET setup as long as they can be gated and coupled to electronic reservoirs [43, 45, 46, 48].

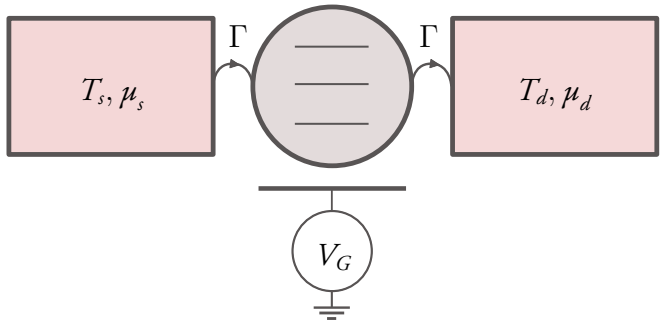

Figure 9: Schematic of a SET where a central QD with discrete energy levels (gray) is coupled to two electronic reservoirs, source and drain, with well-defined temperatures and chemical potentials. A third contact, the gate, is used to change the electric potential of the QD by an applied voltage V_G. The QD is tunnel coupled to the reservoirs such that the mean rate for electron tunneling is given by Γ.

The transport properties of a SET depend heavily on the energetics of the many body electron states of the QD. We will therefore start by discussing a simple model used to determine these energies. For this it is assumed that the energies of the single particle states are determined by the confinement alone, as discussed in section 2.4, and do not depend on the overall potential or the charge of the QD. This is of course a crude approximation, but will be sufficient to get a general picture of the energetics. Strong electron-electron interactions require care when putting several electrons on the QD. A commonly employed model for describing the many body energy spectrum is the constant interaction model, which is a classical electrostatic model where the energies are calculated from capacitances and charges [59, 60]. This is can be motivated by the fact that the reservoirs, gate and QD are all (fairly) conducting materials in close proximity to one another. It is thus possible to associate a finite capacitance to each junction between them. If the capacitances between the different contacts are ignored, the electrostatic potential of the QD with net charge Q can be calculated as

$$V_{QD}(Q) = \frac{1}{C_\Sigma}\left(Q + \sum_{j=s,d,g} V_i C_j\right), \tag{27}$$

where V_j is the applied voltage (i.e. electrical potential) to contact j, C_j is the capacitance between j and the QD and $C_\Sigma = \sum_{j=s,d,g} C_j$. $j = s, d, g$ corresponds to the two electron reservoirs, source and drain, as well as the gate, respectively. From Eq. 27 it is then possible to calculate the electrostatic energy of a QD with net charge $-eN$ (i.e. N excess electrons)

$$U(N) = \int_0^{-eN} V_{QD}(Q)dQ = \frac{e^2N^2}{2C_\Sigma} - eN\left(\sum_{j=s,d,g}\frac{C_j}{C_\Sigma}V_j\right). \tag{28}$$

Using the constant interaction model the energy for a N electron state can thus be expressed as

$$E(N) = \sum_i \varepsilon_i + U(N), \tag{29}$$

where ε_i is the energy of an occupied single particle state. From Eq. 29 it is straight-forward to obtain the energy $\tilde{\mu}$ needed to add an electron to the QD, which will be referred to as a chemical potential. For example, the chemical potential for adding an electron to single particle state i, if there already are $N-1$ electrons on the QD is

$$\mu_{N,i} = \varepsilon_i + E_C\left(N - \frac{1}{2}\right) - e\alpha_G V_G, \tag{30}$$

if any bias voltage is applied symmetrically to the source and drain ($V_s = -V_d$). $\alpha_G = \frac{C_G}{C_\Sigma}$ is commonly referred to as the gate lever arm and $E_C = \frac{e^2}{C_\Sigma}$ as the charging energy. If the single particle orbitals are spin-degenerate the difference in $\tilde{\mu}$ for adding the first electron (e.g. spin up) and second electron (spin down) is

$$\Delta\tilde{\mu}_i = \tilde{\mu}_{N+1,i,\downarrow} - \tilde{\mu}_{N,i,\uparrow} = E_C. \tag{31}$$

A large charging energy will have very pronounced effects on the transport characteristics of a SET [60, 61]. This can be understood from the energy diagram in the Fig. 10.a where $E_C \gg k_B T$ and only a single spin-degenerate orbital is assumed to be within reach for electrons in the reservoirs. It is then only possible to have electron exchange between the QD and a reservoir when $\tilde{\mu}$ of the QD lies within a few $k_B T$ of μ in the reservoir (set by the thermal broadening of the Fermi-Dirac distribution), as any transition requires a filled initial and empty final state. The device is put in a current-carrying state when the following two conditions are satisfied: the total system needs to be put out of equilibrium, e.g. by introducing a difference in μ and/or T between the source and drain; $\tilde{\mu}$ is located at an energy where the non-equilibrium conditions create a population imbalance of electrons in the reservoirs, as in Fig 10.a. Furthermore, in the current-carrying state the electron number on the QD fluctuates between $N \leftrightarrow N+1$, and electrons will be transported between the reservoirs one by one (assuming the tunnel rate Γ is small), as the large E_C makes it energetically forbidden to add two charges to the QD. Hence the name single electron transistor. The conductance $G = \frac{dI}{dV_{sd}}$ of a SET at low T will have a very characteristic line-shape [60], which can be observed in Fig. 10.b where G is plotted against V_G for $V_{sd} = 0$. There is a clear peak in the conductance whenever a chemical potential of the QD aligns with μ of the reservoirs. In between the peaks, i.e. several $k_B T$ away, the large E_C makes it impossible to drive any current though the device, a phenomenon known as Coulomb blockade, and oscillations in the conductance is a clear indication that a device is in the Coulomb blockade regime.

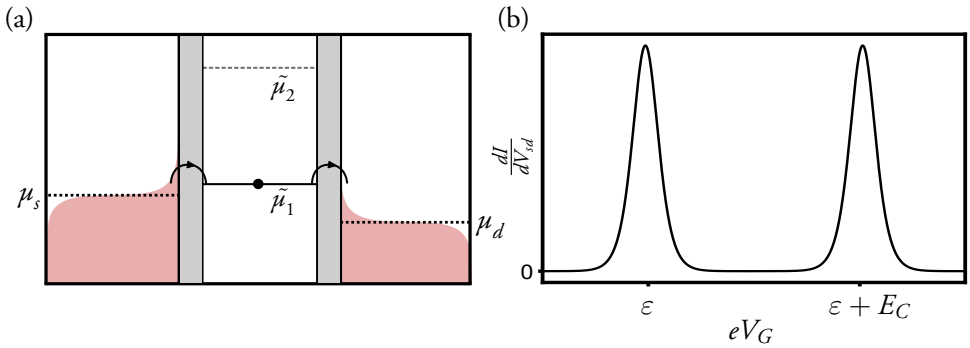

Figure 10: a) Energy diagram illustrating transport in a QD-based SET with large level splitting such that only one spin-degenerate orbital is available for transport. The discrete energy states of the QD, the central region, limits transport to as little as a single energy. The colored regions correspond to the Fermi-Dirac distributions of the reservoirs. Non-equilibrium conditions are created by an applied voltage $eV_{sd} = \mu_s - \mu_d$, where μ_s and μ_d are the chemical potentials of the source and drain, respectively. The chemical potentials for adding the first electron, $\tilde{\mu}_1 = \varepsilon - e\alpha_G V_G$, and the second electron, $\tilde{\mu}_2 = \varepsilon - e\alpha_G V_G + E_C$, to the QD differ by E_C. b) The zero-bias conductance of a Coulomb blockaded QD shows clear peaks whenever the chemical potential of the QD lies within a few $k_B T$ of μ of the reservoirs. The figure is based on calculations where the QD can accommodate a maximum of one electron with each spin, where $E_C = 100 k_B T$ and $\alpha_G = 1$.

When the first and second electron are put in single particle states with the same energy, e.g. in a spin-degenerate orbital, the distance between the peaks is equal to E_C, making it a parameter that is easily determined in an experiment.[3] For QDs with several orbitals the frequency of the oscillations is not constant, and not all distances between conductance peaks correspond to E_C [62]. However, the experimental devices used in papers I and II can be accurately modeled as having a single spin-degenerate orbital, and effects originating from having more than one orbital will not be discussed further.

In the preceding discussion it was assumed that electrons are transported only at a single energy set by $\tilde{\mu}$ of the QD. This is a valid description as long as the barriers separating the QD and its reservoirs are large, and tunneling remains an unlikely event. In that case the transport problem (i.e. calculating currents) can be solved using Fermi's golden rule based on leading order perturbation theory in the tunnel coupling Γ [63]. However, for larger Γ electrons can be transported across the QD at a comparatively fast rate. This leads to an uncertainty in the energy of transported electrons according to the uncertainty principle

$$\Delta E \cdot \Delta t \geq \frac{\hbar}{2}, \tag{32}$$

as the temporal uncertainty Δt for time spent on the QD becomes small. Taking into account the energy uncertainty, as well as a large E_C, when modeling transport in QD devices is not trivial, as will be evident in the following section.

[3] This is exactly true for SETs based on metallic islands. But for a QD with a spin-degenerate orbital the peak position will be shifted by a small amount $\sim k_b T \ln \sqrt{2}$ [60].

4 Real time diagrammatic technique

When setting up the transport theory below, the abstraction level of the device needs to be increased by one step, and we will consider an arbitrary QD-like object tunnel coupled to any number of metallic contacts, which act as fermionic reservoirs. By having different chemical potentials (by means of applying a voltage) or temperatures (by means of heating) of the reservoirs currents can flow between them by going through the QD. The current will then naturally be heavily influenced by the properties of the QD, as was exemplified in the previous section. Typical for such systems is that the total system (QD plus reservoirs) has so many degrees of freedom that a full quantum mechanical description, i.e. solving the Schrödinger equation for the full system, becomes insurmountable. The common way to avoid this problem is to assume that the reservoirs contain enough (non-interacting) particles to always be in an equilibrium state characterized be the Fermi-Dirac distribution in Eq. 11. It is then sufficient to only solve for the state of the QD in order to calculate transport.

There exist many techniques for calculating transport in these systems, all of which has their limitations, and the most appropriate approach is chosen based on the properties of the device to be modeled. If, for example, electron-electron interactions on the QD are so small that they can be neglected the transport problem can be solved exactly using Landauer-Büttiker theory [64, 65]. If instead the interactions are fairly small, but not negligible, and the tunnel coupling to the reservoirs strong ($E_C < \hbar\Gamma$), non-equilibrium Green's function techniques are commonly used [66, 67]. When $\hbar\Gamma \sim E_C$ the problem is usually tackled using renormalization-group techniques [68]. For systems where the tunnel coupling is very weak master equation techniques are common tools [69]. These are based on a perturbative expansion in $\hbar\Gamma$ and have the benefit of being able to treat electron-electron interactions exactly. Since the experimental devices used in papers I and II consist of QDs weakly coupled to reservoirs, and where the electron-electron interactions can become very large, it was well motivated to use a master equation approach to model these devices. There are several master equation techniques available, but for these projects the choice fell on the real time diagrammatic (RTD) technique. The name hints at the fact that diagrams are a part of the formulation and that the calculations are being performed in real time, as opposed to along an imaginary time axis. This technique is an appropriate choice because also second order tunneling effects ($\propto \Gamma^2$) needs to be included to model the experimental devices, something that is not commonly done. The RTD theory provides a systematic expansion in $\hbar\Gamma/k_B\mathrm{T}$ without the need to artificially insert a life-time broadening of electrons on the QD to account for an energy uncertainty of transported electrons, which is needed for its strongest contender; the T-matrix approach [70]. The technique was originally developed in Refs. 71–73 using Keldysh contours. It was later reformulated using Liouville supero-perators [74–76], with the benefit that the number of diagrams one needs to keep

track of is drastically reduced, making numerical implementations more straight-forward. There exist formulations of the technique both in time and in Laplace (frequency) space, and it has now been used to study a variety of different problems ranging form, for example, time-dependent decay problems [77], to transport in systems with superconducting leads [78] or where spin-physics becomes important [79–81]. In this thesis we will stick to stationary state solutions, for which the state-or-art progress includes being able to calculate energy currents up to order Γ^2 [82, 83], and being able to study Kondo physics using a renormalization group theoretical approach [84].

Below follow the main steps of a derivation of generalized master equations using the RTD technique, based primarily on Refs. 76 and 83, as well as some tips and tricks that increases the efficiency of a numerical implementation. For the remaining part of this chapter it is assumed that the reader is familiar with the concepts of second quantization and density matrices.

4.1 Model system

Figure 11 shows a schematic picture of a quantum object coupled to three reservoirs, with whom it can exchange particles and energy (illustrated by the arrows).

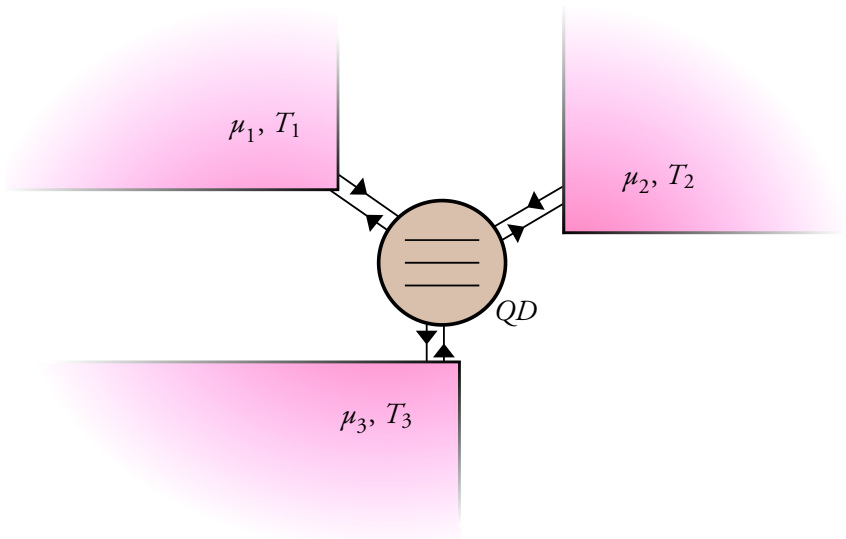

Figure 11: Standard system for studying transport through QDs. The QD (center object) is tunnel coupled to macroscopic electron reservoirs. The reservoirs are each assumed to be in local thermal equilibrium and can thus be characterized by a chemical potential μ and a temperature T. Transport is driven by having different chemical potentials and temperatures in the reservoirs.

The goal of the theoretical modeling using the RTD theory is to calculate electronic transport through QDs, that is we limit the QD to accommodate only fermions. To set up

the theory one starts with a Hamiltonian description of the QD and its reservoirs. The general Hamiltonian for the total system is given by the sum of the Hamiltonians for the subsystems

$$H = H_D + \sum_r H_r + \sum_r H_{T,r} = H_D + H_R + H_T. \tag{33}$$

Here, H_D is the Hamiltonian describing the QD, which on diagonal form simply reads

$$H_D = \sum_a E_a |a\rangle\langle a|, \tag{34}$$

where $|a\rangle$ is a many body eigenstate of the isolated QD and E_a is its energy. A non-interacting fermionic reservoir r is described by

$$H_r = \sum_{k,\sigma} \omega_{k,\sigma,r} c^\dagger_{k,\sigma,r} c_{k,\sigma,r}, \tag{35}$$

where $\omega_{k,\sigma,r}$ is the eigenenergy for a state in reservoir r with single particle index k and spin σ. The field operators acting on a reservoir subspace are denoted by the letter c.

The Hamiltonian describing electron tunneling between the QD and a reservoir is modeled by the bi-linear Hamiltonian

$$H_{T,r} = \sum_{k,\sigma,j} t_{k,\sigma,r,j} d^\dagger_{\sigma,j} c_{k,\sigma,r} + h.c.\ , \tag{36}$$

with j labelling the different single particle orbitals of the QD and $d^\dagger(d)$ denotes field operators acting on the QD subspace. The amplitude for electron tunneling is given by $t_{k,\sigma,r,j}$, which allows us to define a tunneling rate

$$\Gamma_{k,\sigma,r,j} = \frac{2\pi\nu_r |t_{k,\sigma,r,j}|^2}{\hbar}. \tag{37}$$

Here ν_r is the density of states of the reservoir and in the sections to come we utilize the wide band approximation assuming that ν_r is constant over an energy D much larger than any other involved energy scale, motivated by its weak energy dependence inside the bands of bulk metals, see Fig. 5. For convenience we also set $\hbar = e = k_B = 1$.

4.2 Liouville space super-operators

In order to use real time diagrammatics to derive generalized master equations we need to define convenient super-operators in Liouville space whose properties resemble those of fermionic field operators in Hilbert space so that Wick's theorem can be applied also to the

super-operators. Using such operators, it is possible to rewrite the Hamiltonians in the previous section and perform a perturbative expansion of the tunneling coupling in Liouville space.

First, a note about a compact notation that will be used throughout the derivation. The fermionic creation and annihilation operators acting on the QD Hilbert subspace will be written as

$$d_{\eta\sigma j} = \begin{cases} d_{\sigma,j} & \text{if } \eta = - \\ d^\dagger_{\sigma,j} & \text{if } \eta = + \end{cases}, \tag{38}$$

i.e. η is the electron-hole index. All indices are then combined to a single index represented by a positive integer, $1 = \eta_1\sigma_1 j_1$, and a bar denotes the sign change of appropriate numbers i.e. $\bar{1} = \bar{\eta}_1\sigma_1 j_1 = (-\eta_1)\sigma_1 j_1$ and later $\bar{q}_1 = -q_1$. Furthermore, a sum over such a multi-index ($\sum_1$) is implicitly understood as sums over all involved indices.

Using the definition in Eq. 38 we follow Ref. 76 and introduce super-operators acting on the QD subspace

$$\mathcal{G}_1^{q_1}\bullet = \frac{1}{\sqrt{2}}(d_1 \bullet + q_1(-1)^{N_D} \bullet (-1)^{N_D} d_1), \quad q_1 \in \{-,+\}, \tag{39}$$

with $N_D = \sum_\sigma n_\sigma = \sum_{\sigma,j} d^\dagger_{\sigma,j} d_{\sigma,j}$, and $\bullet$ represents an arbitrary operator. These operators have properties similar to those of fermionic operators in Hilbert space

$$(\mathcal{G}_1^{q_1})^\dagger = \mathcal{G}_{\bar{1}}^{\bar{q}_1}, \tag{40}$$

$$[\mathcal{G}_2^{q_2}, \mathcal{G}_1^{q_1}]_+ = \delta_{q_2\bar{q}_1}\delta_{2\bar{1}}\mathcal{I}, \tag{41}$$

where $[..]_+$ is the anticommutator. Analogously, the field operators acting on the reservoir subspace are defined in the same way and denoted $\mathcal{J}_1^{q_1}$, where the reservoir index r is also included in the multi-index.

A Liouville super-operator is defined as $L_X\bullet \equiv [H_X, \bullet]_-$. Using the definition of L together with Eq. 39 one can translate the system's total Hamiltonian from section 4.1 to Liouville form as

$$L = L_D + L_T + L_R \tag{42}$$

$$L_D = [H_D, \bullet]_- \tag{43}$$

$$L_R = [H_R, \bullet]_- = \sum_1 \eta_1\omega_1 \mathcal{J}_1^+ \mathcal{J}_{\bar{1}}^- \tag{44}$$

$$L_T = [H_T, \bullet]_- = \sum_1 t_{1'1}\eta_1 \sum_{q_1} \mathcal{G}_{1'}^{\bar{q}_1} \mathcal{J}_{\bar{q}_1}^{q_1} \tag{45}$$

where $t_{1'1} = \delta_{r_{1'}r_1} t_1$.

4.3 Generalized master equations

The starting point for deriving generalized master equations that can be used to calculate transport through a QD is the Liuoville-von Neumann equation. It is the differential equation that describes the time evolution of the full system density matrix, which in the Schrödinger picture reads

$$\frac{d}{dt}\rho = -i[H,\rho]_- = -iL\rho. \tag{46}$$

Equation 46 has the formal solution

$$\rho(t) = e^{-iLt}\rho(0), \tag{47}$$

from which it is possible to obtain the reduced density operator of the QD ρ_D by tracing out the reservoir degrees of freedom

$$\rho_D(t) = \underset{R}{\mathrm{Tr}}\rho(t). \tag{48}$$

We assume that the reservoir density matrix ρ_R and ρ_D are uncorrelated at time $t_0 = 0$, i.e. $\rho(0) = \rho_D(0)\otimes\rho_R$, and that L is time independent. Then, Laplace transforming equation 48 yields

$$\begin{aligned}\rho_D(z) = \underset{R}{\mathrm{Tr}}\int_0^\infty e^{izt}e^{-iLt}\rho(0)dt &= \underset{R}{\mathrm{Tr}}\frac{i}{z-L}\rho_D(0)\otimes\rho_R \\ &= \underset{R}{\mathrm{Tr}}\frac{i}{z-L_D-L_R-L_T}\rho_D(0)\otimes\rho_R.\end{aligned} \tag{49}$$

The quotient is then expanded in L_T to obtain the geometric series

$$\frac{i}{z-L_D-L_R-L_T} = \frac{i}{z-L_D-L_R} + \frac{i}{z-L_D-L_R}(-iL_T)\frac{i}{z-L_D-L_R-L_T}. \tag{50}$$

Using normalization conditions $\underset{R}{\mathrm{Tr}}L_R = 0$ and $\underset{R}{\mathrm{Tr}}\rho_R = 1$, together with Eq. 50 makes it possible to express equation 49 as [76]

$$\rho_D(z) = \Big[\frac{i}{z-L_D} + \frac{i}{z-L_D}\sum_k\Big(-iW(z)\frac{i}{z-L_D}\Big)^k\Big]\rho_D(0), \tag{51}$$

where

$$W(z) = \sum_{k=1}^{\infty}\underset{R}{\mathrm{Tr}}\Big(L_T\frac{1}{z-L_D-L_R}\Big)^k L_T\rho_R\Big|_{irred.}. \tag{52}$$

irred here refers to the irreducible diagrams in the perturbative series. A diagram is irreducible if it cannot be factorized into lower order diagrams separated by a free propagation

term $\frac{i}{z-L_D}$. For a graphical representation of the irreducible series the reader is encouraged to consult Refs. 73–75. By identifying Eq. 51 as a geometrical series we can rewrite it as

$$\rho_D(z) = \frac{i}{z - L_D - W(z)}\rho_D(0), \tag{53}$$

and by re-arranging the terms we get

$$iz\rho_D(z) - \rho_D(0) = (-iL_D + W(z))\rho_D(z). \tag{54}$$

This allows us to identify the left-hand side as the time derivative, and we can thus obtain the stationary state density matrix by taking the zero-frequency limit ($z \to i0^+$), arriving at the generalized Master equations for the reduced density matrix of the QD,

$$0 = (-iL_D + W)\rho_D. \tag{55}$$

4.4 Kernel evaluation

Solving Eq. 55 for ρ_D provides an exact solution to Eq. 46 as long as all terms in equation 52 are included. However, keeping terms beyond leading order in the expansion is cumbersome and quickly becomes impossible from a practical point of view. Only terms of even order in k give a non-vanishing contribution, and it is common to perform a systematic expansion up to order $k = 2$ ($\propto \Gamma$), and sometimes $k = 4$ ($\propto \Gamma^2$), as will be done here. Even higher order terms can to some degree be included in the resonant tunnel approximation [71–73], in which a subset of these terms are kept, or when using real time diagrammatics in a renormalization group approach [75, 76].

When evaluating W the reservoir degrees of freedom are traced out by collecting all reservoir super-operators and calculating their expectation values using Wick's theorem

$$\langle \mathcal{J}_n^{q_n} \mathcal{J}_{n-1}^{q_{n-1}} \dots \mathcal{J}_1^{q_1} \rangle_R = \sum_P (-1)^P \prod_{\langle i,j \rangle} \langle \mathcal{J}_j^{q_j} \mathcal{J}_i^{q_i} \rangle_R \tag{56}$$

where P is the number of permutations needed to create the pairs of operators $\langle i, j \rangle$ on the right hand side, and

$$\langle \mathcal{J}_2^{q_2} \mathcal{J}_1^{q_1} \rangle_R = \delta_{q_2-} \left(\delta_{q_1+} + \delta_{q_1-} \tanh\left(\frac{\eta_1(\omega_1 - \mu_1)}{2T_1} \right) \right) \equiv \gamma_1^{q_1}. \tag{57}$$

The leading order terms of the kernel can now be written

$$W^{(2)} = \sum_{1 q_1} \frac{\Gamma_1}{2\pi} \mathcal{G}_{\bar{1}}^{+} \frac{q_1 \gamma_1^{q_1}}{i0 - L_D + \eta_1 \omega_1} \mathcal{G}_1^{\bar{q}_1}, \tag{58}$$

and the next to leading order is given by [74, 81, 82]

$$W^{(4)} = \sum_{12q_1q_2} \frac{\Gamma_1\Gamma_2}{(2\pi)^2} \left(\mathcal{G}^+_{\bar{1}} \frac{1}{\eta_1\omega_1 + i0 - L_D} \mathcal{G}^+_{\bar{2}} - \mathcal{G}^+_{\bar{2}} \frac{1}{\eta_2\omega_2 + i0 - L_D} \mathcal{G}^+_{\bar{1}} \right) \times \frac{\bar{q}_2\gamma_2^{\bar{q}_2}}{\eta_1\omega_1 + \eta_2\omega_2 + i0 - L_D} \mathcal{G}_2^{q_2} \frac{\bar{q}_1\gamma_1^{\bar{q}_1}}{\eta_1\omega_1 + i0 - L_D} \mathcal{G}_1^{q_1}. \tag{59}$$

The physical processes described by $W^{(4)}$ correspond to coherent events in which two tunneling processes take place in a short time interval. This can e.g. transport electrons across the QD through brief population of virtual intermediate states temporarily violating energy conversion, as allowed by the Heisenberg uncertainty principle. Including these terms thus results in a broadened energy distribution of transported electrons and a finite current can be found also in the Coulomb blockade regime.

The matrix elements of a super-operator A are evaluated as

$$A^{ab}_{cd} = \langle c| \Big(A|a\rangle\langle b| \Big) |d\rangle. \tag{60}$$

When evaluating the matrix elements of W using 58 and 59 one encounters several integrals. The solutions to these integrals are given in Refs. 74 and 82 for $T_1 = T_2$, and in the supporting material of Ref. 81 for the case when $T_1 \neq T_2$.

4.5 Observables

Any observable can now be calculated using the density matrix[4]

$$\langle A \rangle = \mathrm{Tr}(A\rho) = \frac{1}{2}\mathrm{Tr}\,(L_A^+\rho), \quad L_A^+ \bullet = [A, \bullet]_+. \tag{61}$$

When modeling heat engines we are primarily interested in two observables, the charge and energy current. The charge current leaving reservoir r can be obtained from the time derivative of the particle number in the reservoir ($e = 1$)

$$I_r = \frac{d}{dt} N_r = i[H, N_r]_-, \quad N_r = \sum_{q,\sigma} c^\dagger_{q,\sigma,r} c_{q,\sigma,r}. \tag{62}$$

However, instead of calculating $\frac{d}{dt}N_r$ directly, the evaluation of the particle current can be simplified using the fact that the charge (and thus number of particles) is conserved in all tunneling processes

$$[H_{T,r},\ N_r + N_D]_- = 0. \tag{63}$$

[4]This follows from the cyclic property of the trace, $\mathrm{Tr}(AB) = \mathrm{Tr}(BA)$.

This conservation law allows us to calculate the number of particles entering the QD from the reservoir instead of calculating the number of particles leaving the reservoir when evaluating the current. By using the charge conservation together with equation 61 one can express the charge current as [76]

$$I_r = i\,\mathrm{Tr} L^+_{N_D} W_r \rho_D, \tag{64}$$

where W_r is similar to W in equation 52 with the only difference being that the left-most L_T is replaced by $L_{T,r}$. This leads to great numerical simplifications as $W = \sum_r W_r$ is already calculated when solving for ρ_D. Thus no additional kernel is needed and unnecessary integral evaluations are avoided.

A similar treatment is possible for the energy current, defined as the energy change of a reservoir, but one needs to be careful since the energy flowing out of a reservoir is not necessarily equal to the energy entering the QD from the same reservoir (although the total energy is always conserved) [85]

$$[H_{T,r},\ H_r + H_D]_- \neq 0. \tag{65}$$

Instead the energy change in reservoir r can be rewritten

$$[H_{T,r},\ H_r] = -[H_{T,r},\ H_D] - [H_{T,r}, \sum_{r'} H_{T,r'}] + [H_{T,r},\ H] \tag{66}$$

where $r \neq r'$. The right-most term can be identified as the time-dependent change of $H_{T,r}$, which can lead to a temporary energy storage in the barriers if the Hamiltonian is time dependent [86], but will vanish in the stationary limit of interest here. This means that instead of calculating the energy observable directly in the reservoir we can evaluate it from the two terms, one describing the energy change in the QD due to the coupling to reservoir r, $[H_{T,r},\ H_D]$, and one associated with the tunnel couplings, $[H_{T,r}, \sum_{r'} H_{T,r'}]$. By expressing these parts using the Liouville formalism one can obtain [83, 87]

$$J_{E_r} = i\underset{D}{\mathrm{Tr}} L^+_{H_D} W_r \rho_D - i\underset{D}{\mathrm{Tr}} W_{\Gamma,r} \rho_D. \tag{67}$$

Here the first term on the right-hand side is evaluated in the same manner as Eq. 64, and the second term is given by

$$W_{\Gamma,r} = \underset{R}{\mathrm{Tr}} L^+_{T,r} L_T \Big(\frac{1}{z - L_D - L_R} L_T \Big)^k \rho_R \Big|_{irred.}. \tag{68}$$

The leading order contribution of this term will be proportional to Γ^2 and as a result it does not contribute when considering only first order processes. In order $\propto \Gamma^2$ the kernel

$W_{\Gamma,r}$ is given by[5] [83, 87]

$$\begin{aligned}\underset{D}{\mathrm{Tr}} W^{(4)}_{\Gamma,r} = &\sum_{\substack{1,2,j \\ r=r_1, r_1\neq r_2}} \frac{-i\Gamma_2^{j,j_2}\Gamma_1^{j,j_1}}{4\pi} \underset{D}{\mathrm{Tr}}\mathcal{G}_1^- \frac{\gamma_1^-}{-\eta_1\omega_1 + i0 - L_D}\mathcal{G}_2^+\delta_{\sigma_1,\sigma_2}\delta_{\eta_1,\bar{\eta}_2} - \\ &\sum_{\substack{1,2,j \\ r=r_2, r_1\neq r_2}} \frac{-i\Gamma_2^{j,j_2}\Gamma_1^{j,j_1}}{4\pi} \underset{D}{\mathrm{Tr}}\mathcal{G}_1^- \frac{\gamma_1^-}{-\eta_1\omega_1 + i0 - L_D}\mathcal{G}_2^+\delta_{\sigma_1,\sigma_2}\delta_{\eta_1,\bar{\eta}_2}\end{aligned}, \tag{69}$$

where $\Gamma_1^{j,j_1} = 2\pi\nu_{r_1} t_{\sigma_1,r_1,j} t_{\sigma_1,r_1,j_1}/\hbar$.

As with the charge current there will be numerical gains from using the conservation laws to obtain the energy current according to equation 67. If J_{E_r} is evaluated inside a reservoir a new kernel must be set up where the evaluation of matrix elements requires solving double integrals without known analytical solutions. When calculating J_{E_r} as described in this section W_r is then already calculated when solving for ρ_D, and in addition the integrals needed when setting up $W_{\Gamma,r}$ are analytically solvable, one dimensional integrals very similar to those used in Eq. 58.

The expressions given in this section describe the calculation of charge and energy current, from which the heat current is obtained through the first law of thermodynamics

$$J_{Q_r} = J_{E_r} - \frac{\mu_r}{e} I_r. \tag{70}$$

5 Lindblad master equation

A master equation can only generate density matrices that represent physical systems if it is a trace preserving and completely positive map, which is not guaranteed in most techniques. Trace preservation ensures that $\mathrm{Tr}\rho = 1$, i.e. probability normalization, at all times, whereas complete positivity results in the density matrix only having positive numbers on its diagonal. In ρ these numbers correspond to the probability of the system being in different states and negative values have no physical meaning. ρ calculated using the RTD theory in the previous section will always have the correct trace, but negative probabilities can occur.

[5]The trace is always present in the calculations and is included here since it has been used to simplify the expression.

The most general form of master equation that always yields a physical density matrix is the (time dependent) Lindblad master equation[6] [89]

$$\frac{d\rho_D}{dt} = -i[H_D(t), \rho_D(t)]_- + \sum_i \left(A_i(t)\rho_D(t)A_i^\dagger(t) - \frac{1}{2}\left[A_i^\dagger(t)A_i(t), \rho_D(t)\right]_+ \right), \quad (71)$$

which can also account for non-unitary evolution, e.g. the inclusion of dissipative processes. Here $A_i(t)$ are the collapse, or jump, operators accounting for the physical processes one wishes to include, which will be different for each problem. Problems that are well suited for the Lindblad equation includes a QD coupled to an environment where energy exchange induces stochastic jumps between different energy levels, as will be the case in paper III.

When deriving Eq. 71 (see e.g. Ref. 90) the following assumptions are commonly made (which limits its applicability to a subset of possible problems). The density matrix is assumed to be separable at $t = 0$, i.e. $\rho(0) = \rho_D(0) \otimes \rho_R$ and the system-environment coupling is assumed to be weak so that the state of the environment remains constant and the density matrix is approximately separable at all times. Furthermore, the Markov approximation is used where the relaxation time of the environment is much shorter than that of the QD. Finally, the secular approximation needs to be fulfilled, i.e. the smallest energy separation between non-degenerate states is larger than the coupling to the environment. These conditions are very similar to those used when setting up the RTD theory where the separability and Markov approximations are always valid. When only leading order terms in Eq. 52 are kept and the secular approximation is imposed the RTD master equations will even be of Lindblad form.

[6] It is also known as the GKSL equation after Gorini, Kossakowski, Sudarshan [88] and Lindblad.

Thermoelectric engines

A thermoelectric device is a heat engine in the sense that it can convert thermal energy into useful electrical energy. It does, however, not belong to the same category of engines as its cyclic counterparts discussed in the introduction, but is instead classified as a particle-exchange heat engine [91]. Engines in this class do not use a working gas, but operate by continuously exchanging particles directly between the reservoirs. Its operation relies on some mechanism making the particle transport energy selective, and work is extracted when the particles move against some field increasing their potential energy. The engines can in theory be operated reversibly, and reversibility is found when the particle transfer is isentropic, requiring that all matter and energy flows vanish [92, 93]. As a consequence, reversibility is only possible when there is a tight coupling between charge and heat flow, resulting in completely interdependent currents that vanish at the same time [94]. This requirement makes QDs excellent candidates for reversible solid-state generators, as will be discussed later in this chapter. The chapter begins with an introduction to the thermoelectric effects in bulk materials as well as nanostructures, and ends with summaries of papers I and II in which QD-based thermoelectric generators are studied.

6 Traditional thermoelectrics

The thermoelectric effects describe interconnections between a material's electrical and thermal properties. The effects are three in total; the Seebeck effect, the Peltier Effect and the Thomson effect. The Seebeck effect bears the name of Thomas Seebeck who discovered that a persistent current runs through a closed electric circuit consisting of two dissimilar conductors joined at two places if one of the junctions is heated[7] [96]. If the conductors are only joined in a single place such that the electrical circuit is not closed, and this junction is heated, an open circuit voltage is generated. It was soon identified that this effect does not require two conductors but is present also in standalone materials where a temperature

[7]Although the discovery is attributed to Seebeck, it was actually first discovered by Alessandro Volta who found that he could induce muscle twitches in dead animals using a metallic rod with one of its ends heated [95].

difference, or gradient, generates a difference in electric potential. The magnitude of this effect is quantified using the Seebeck Coefficient

$$\alpha = \frac{\Delta V}{\Delta T}\bigg|_{\mathrm{I}=0}, \tag{72}$$

relating the generated voltage ΔV to the temperature bias ΔT for a vanishing charge current I. The next effect, the Peltier effect, is the inverse of the Seebeck effect where a voltage or current through a conductor generates a temperature difference, i.e. transports heat [97]. In time-reversal symmetric systems, e.g. where no external magnetic field or magnetic ordering is present, the Peltier coefficient is given by

$$\Pi = \alpha T. \tag{73}$$

The third effect, the Thomson effect, is a continuous version of the Peltier effect present when a temperature gradient results in a gradient of α, as it generally depends on T. The Thomson coefficient measures the rate of local heating resulting from an inhomogeneous Seebeck coefficient [98]

$$\mathcal{K} = T\frac{\nabla \alpha}{\nabla T}. \tag{74}$$

In this chapter only energy harvesting, i.e. converting thermal energy to electrical energy, is of interest and of the three effects only the Seebeck effect is relevant. The others will not be discussed further.

6.1 Linear response

When modeling transport properties of bulk materials, be it electric or thermoelectric, it is very common to use linear response theories in which non-equilibrium conditions are taken into account by expanding to linear order around the local equilibrium. This is a good approach whenever ΔV and ΔT is small compared to the overall temperature T. Within a linear response description the charge current is given by

$$I = G \cdot \Delta V + \alpha G \cdot \Delta T, \tag{75}$$

where $G = \frac{\Delta I}{\Delta V}\big|_{\Delta T=0}$ is the linear conductance. The validity of linear response can sometimes be questioned, e.g. for thermoelectric generators which can operate at $\Delta T \sim T \sim$ 300K, but it holds surprisingly well for bulk materials. This can be explained by considering the short relaxation lengths of the charge carriers inside these materials. Crucial for a linear response treatment is that the carrier distributions should not deviate much from equilibrium distributions. The short relaxation length, on the order to the mean free path $\sim$ 100 nm, compared to the generator's macroscopic size ensures that the carriers always stay close to equilibrium. Thus, as long as $\Delta T \ll T$ on the on the order of the mean

free path a linear response treatment can be motivated [99]. It will, however, break down in nanoscale systems whose sizes are smaller than a typical electron mean free path, and a non-linear treatment based on a complete microscopic description of the system is often necessary. In the research presented in this chapter linear response is not assumed, although paper II explores how well such a treatment would work for a QD-based thermoelectric device.

Since Eq. 75 is almost always valid for bulk materials it has become common practice to measure the thermoelectric performance using only linear response quantities. Typically, it is quantified using the dimensionless figure of merit

$$ZT = \frac{\alpha^2 GT}{\kappa}, \tag{76}$$

in which κ is the thermal conductance relating the heat flux J_Q to the temperature difference $\kappa = \kappa_{el} + \kappa_{ph} = \frac{J_Q}{\Delta T}\big|_{I=0}$, with contributions from both charge carriers and phonons. A large ZT corresponds to high performance of a thermoelectric element, and ideal performance, i.e. a Carnot efficient engine, is found when $ZT \to \infty$. However, in systems where a linear response description is invalid ZT can no longer be used as a reliable measure of engine performance [100–102], and one is best to resort to other means of measuring performance. For example using the power and efficiency.

6.2 Bulk thermoelectrics

Maximizing ZT in Eq. 76 requires increasing α and G while reducing κ. Unfortunately, this is far from an easy task as all parameters are more or less interdependent. For example, in high conductivity materials $G \cdot \kappa^{-1}$ is constant, a phenomenon known as the Wiedemann-Franz law [103], which makes all improvements to G in order to improve ZT futile. For lower carrier concentrations κ_{ph} starts to dominate the thermal transport [104], which is detrimental for the performance as κ_{ph} is not tied to G and phonons are uncharged quasiparticles that only contribute to a dissipative heat leak.

Even though increasing ZT has proven cumbersome there have been continuous (small) improvements ever since the discovery of thermoelectric materials. The first major leap forward came with the introduction of semiconductors and semiconducting technologies in the 1950s [105]. Prior to that only metals had been considered, which generally exhibit a too weak thermoelectric response to be useful. Thermoelectric elements based on semiconductors found several uses in niche applications throughout the late 20th century. Common for these applications is that robust performance (i.e. low maintenance) and a fast response time have a higher priority than high conversion efficiency, which is the case in e.g. space technologies when solar power is not an option [106]. Thermoelectric ele-

ments have also found some uses in cooling applications where their robustness and lack of moving parts are sought after properties, or where spot-cooling of electronic circuits is needed [107]. The best thermoelectric elements today use semiconductor materials with highly optimized electronic structures and transport properties, and much of the research in the field focus on finding new materials with the best attributes for increasing ZT [108, 109]. State of the art thermoelectric generators today have a ZT-value around 1.5-2.5 [110], and it is believed that they might become a commercially viable option for large scale energy conversion and waste heat recovery when ZT reaches $\sim$ 3-4 [111].

7 Nanoscale thermoelectrics

Thermoelectrics reached the nanoscale in the early 1990s when Hicks and Dresselhaus realized that the electronic structures of quantum wells [112] and quantum wires [113] would be very suitable for increasing the ZT (the underlying mechanisms will be discussed below). In addition, the increased surface and interface area in small systems compared to bulk materials has been shown to be disruptive for phonon transport and thus reduces unwanted heat leaks [114–116]. Some nanoscale systems have the added benefit of being able to violate Wiedemann-Franz law, making it possible to somewhat independently tune the conductance and the thermal conductance of the device, see e.g. Refs. 117-118 and references therein.

7.1 Energy filtering

The principle behind nanoscale systems potentially having good thermoelectric performance is that of energy filtering. Energy filtering relies on unequal transport probabilities of charge carriers at different energies. This is most easily understood using the view of ballistic transport where particles are transported without dissipation, i.e. collisionless transport where the particles do not gain or lose any energy. This picture is not a good description for all nanoscale devices, in particular quantum wells and wires where the mean free path can be shorted than the size of the device, but it is a fairly accurate picture for QDs.

How the actual filtering works can be understood from the examples in Fig. 12 where two macroscopic electronic reservoirs are connected and allowed to exchange particles and energy through a central region whose transport properties account for the filtering. The system in Fig. 12.a transports particles at all energies equally well, and thus performs no filtering at all. As a result, a charge current consisting mostly of high energy electrons flowing from hot to cold is exactly canceled by the charge flow of low energy electrons moving in the opposite direction. However, all particles contribute with a positive amount of heat to the total heat current (c.f. Eq. 70). A temperature difference in this system thus gener-

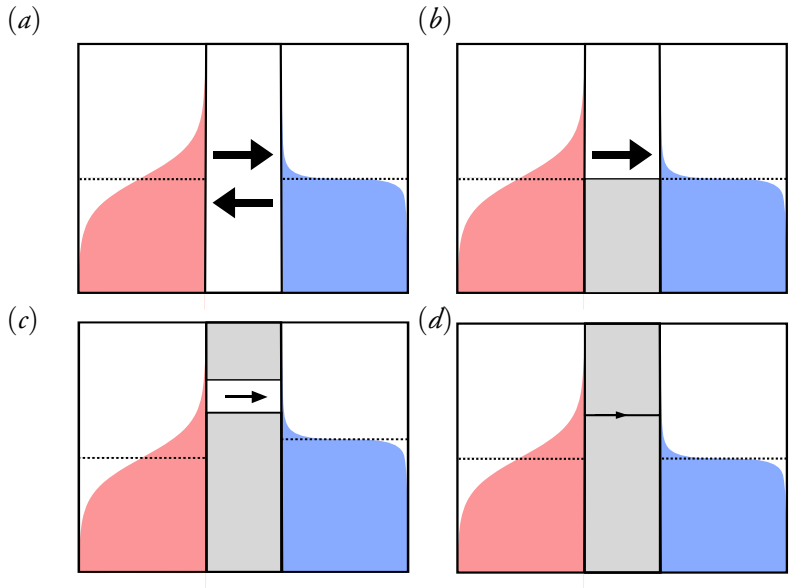

Figure 12: The principle of energy filtering illustrated by considering ballistic electron transport between two reservoirs at different temperatures. The temperature of the red reservoir is higher than that of the blue. The electrons are transported through a central area with transport properties as illustrated in the figure where gray means electron transport is not allowed. The arrows indicate the magnitude and direction of the particle currents. a) No filtering. b) Transport of low energy electrons is blocked. c) Electrons can only be transported in a narrow energy range. In (c) a bias voltage $eV = \Delta\mu$ is included such that the system generates electrical power $P = I \cdot V$. d) Only electrons at a single energy can contribute to the transport.

ates no charge current, but a maximally large heat current, exactly the opposite of what we want. The situation is drastically improved in Fig. 12.b where no transport is allowed below μ of the reservoirs. This yields a large net charge current and the magnitude of the heat current is half of that in the previous example. When used in a thermoelectric generator this system would generate a large output power ($P = I \cdot V$), but at a fairly low efficiency as the large charge current comes at the cost of a large heat current. The heat current will be reduced further in Fig. 12.c where transport is only allowed in a narrow energy band, and thus forbidden also for electrons with a very high energy. This is referred to as a box car transport function, which provides optimal energy filtering if one wishes to maximize the efficiency at a given power [119]. It has been predicted that this transport function can be approximated in e.g. a superlattice of QDs [120–122], in quantum hall devices with energy selective scattering of edge states [123], as well as in an Aharonov-Bohm interferometer [124]. Fig. 12.c also shows how power is generated as it includes a voltage bias forcing the transported electrons to travel electrically "upstream". This increases the electrons' potential energy and electrical work equal to eV is generated per transported electron, highlighting the principle behind thermoelectric energy generation. Finally, in Fig. 12.d the width of the box car function is reduced yielding a delta function. Mahan and Soho [125] showed

that such a delta function yields the highest possible ZT and thus also the highest possible efficiency. As a discrete energy spectrum is the trademark of QDs this created a hope of potentially using them in future thermoelectric energy converters, which we will explore next.

From the principle of energy filtering one can also deduce that 1D and 2D samples should exhibit a strong thermoelectric response since their DOS in Fig. 5 contain parts with strong energy dependences that can be used to filter out unwanted electrons.

7.2 QD thermoelectrics

One of the driving forces behind the fairly large interest in QD thermoelectrics today is the promise of being able to create small, but highly efficient, heat engines and heat pumps [92, 126]. The operating principle of a single QD thermoelectric engine based on a SET is shown in Fig. 13 where it is assumed that the QD couples weakly to its reservoirs limiting electron transport to sequential tunneling. In that case any life-time broadening of the QD orbitals is negligible and electron transport occurs only at energy ε. For the conditions illustrated in the figure there is a net flow of electrons from the hot to the cold reservoir, and each transported electron is associated with an amount of heat $Q_H = \varepsilon - \mu_H$ leaving the hot reservoir. When the electron reaches the cold reservoir a part of Q_H has been used to increase the potential energy of the electron by $eV = \mu_C - \mu_H$, and the remaining energy is deposited as heat in the cold reservoir $Q_C = Q_H - eV = \varepsilon - \mu_C$. Note that this working principle is very similar to that of a traditional heat engine in Fig. 1, with the difference that not only heat, but also particles, are exchanged between the two reservoirs. The efficiency of the engine is given by the ratio of the power output and the heat flowing out from hot reservoir, which in this case is identical to the ratio of the work output and absorbed heat per transported electron, see Eq. 5,

$$\eta = \frac{P}{J_{Q_H}} = \frac{eV}{Q_H} = \frac{\mu_C - \mu_H}{\varepsilon - \mu_H}. \tag{77}$$

Since charge and heat transport are tightly coupled in this setup, i.e. every transported charge is associated with a quantized, fixed, amount of absorbed heat, the QD should be an ideal heat engine and be able to reach the Carnot efficiency [14, 94, 127]. Carnot efficiency requires reversible operation, and thus $\Delta S = 0$, which in a steady-state device means that all flows of matter and heat between the two reservoirs must vanish. Because of the tight coupling between the two they conveniently vanish at the same time. In the device shown in Fig. 13 this requires that the electron distributions of the reservoirs must take the same value at ε. From the Fermi-Dirac distribution in Eq. 11 one can see that this is only possible when

$$\frac{\varepsilon - \mu_H}{T_H} = \frac{\varepsilon - \mu_C}{T_C}. \tag{78}$$

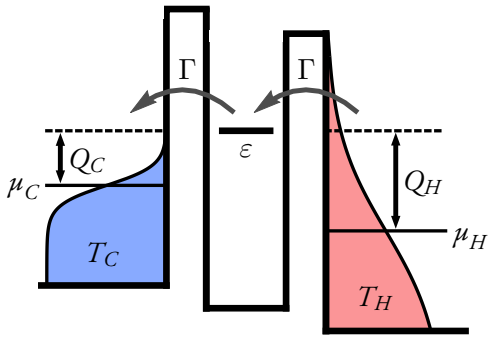

Figure 13: Schematic of a QD heat engine. Every electron transported from the hot to the cold reservoir removes heat Q_H from the hot reservoir and deposits heat Q_C in the cold reservoir if electron transport is limited to a single energy. The difference in absorbed and deposited heat is the work done on the electron when increasing its potential energy by eV, thus converting thermal energy into electrical energy.

Solving for ε and plugging it into Eq. 77 yields $\eta = \eta_C$ [92]. When the QD is instead operated at maximum power its efficiency has been predicted to be close to the Curzon-Ahlborn efficiency[8] η_{CA} introduced in Eq. 8 [13].

The tight coupling between charge and heat flow will be broken when higher order tunneling effects become important, which will increase the heat flow and reduce the maximum efficiency. This is evident from the uncertainty relation in Eq. 32 since the energy of transported electrons is no longer fixed due to a finite life-time of electrons on the QD. An intuitive picture of this mechanism is that the transport function acquires an effective broadening due to the higher order tunneling effects. The effect a finite broadening has on the power and efficiency have been investigated in Refs. 128 and 129 where the tunnel coupling is treated exactly but electron-electron interactions are treated perturbatively, or are ignored. Those studies show that the efficiency decreases with increasing tunnel coupling (and broadening) while the power increases up until $\hbar\Gamma \sim k_B T$, after which the QD starts to lose its energy filtering properties. Since the highest η is reached when electrons are transported only at a single energy η is also reduced when more of the QD states start to contribute to the transport, i.e. when $\Delta\varepsilon$ or $E_C \lesssim k_B T$ [130, 131].

It is worth noting that the preceding argumentation only regards the *electronic* part of the transport. Any phononic flow between the two reservoirs will act as a pure heat leak lowering the efficiency. However, the electronic efficiency is in itself interesting from a fundamental point of view, as well as for practical applications where the electrons are not in equilibrium with their phononic environment [118, 132].

[8]The actual value is slightly higher than η_{CA} due to the non-linear nature of transport in the device.

7.3 Open questions in the field

Much of the early interest in QD thermoelectrics did not regard the potential of high power and efficiency, but rather explaining the outcome of thermoelectric experiments, often focusing on the open circuit voltage or α [133, 134]. Beenakker and Staring were the first to calculate and explain the behavior of α for a QD, which was done in Ref. 60 where they considered a QD with many orbitals and strong electron-electron interactions. By using a sequential tunneling approach they found $\alpha(V_G)$ to have a saw-tooth shape at low temperatures where the periodicity of the oscillations follows that of the Coulomb peaks in the conductance. When instead only a single orbital is included, and E_C is very large, $\alpha(V_G)$ will be a linear function. This can be understood by considering that α is defined for $I = 0$, which requires that the condition in Eq. 78 is fulfilled. Re-arranged the variables in the equation provides a linear relationship between ε and eV. Although this is theoretically sound it does not always describe a physical system particularly well as it would mean an arbitrary large V can be generated at will, and several experiments have observed an $\alpha(V_G)$ that is far from linear [135–137]. The problem was re-tackled in Refs. 138 and 139 where transport is calculated by including both sequential and cotunneling effects. The effective broadening induced by cotunneling processes makes $\alpha(V_G)$ approach zero for large ε, in better agreement with the experiments [140]. However, even though second order tunneling effects are very important for a proper description of a strongly interacting QD close to the open circuit conditions, which is where the efficiency is highest, they are only included in a few cases [135, 138, 139, 141–143]. Usually studies of weakly coupled QDs assume that a sequential tunneling approach is sufficient and that a QD device inherently has a high efficiency. In order to evaluate whether this is a good assumption Paper II explores to which degree the second order effects influence the maximum efficiency and efficiency at maximum power of a single QD heat engine.

Today there exists a large body of theoretical literature on QD thermoelectrics, much of which go beyond considering only a single QD or include also additional physical effects such as magnetism or superconductivity. These works will not be discussed in detail here as the devices used in papers I and II are based on a single QD, but two trends will be commented on. A review of the status of the field from a few years ago can be found in Ref. 144. Many works published since then investigate the thermoelectric performance of multi-QD and multi-terminal devices. The first identified trend is to spatially decouple the charge and heat flow using thermal fluctuations on e.g. a QD or a reservoir to drive a current through another QD [142, 143, 145–152]. The other trend involves studying devices where a hot reservoir is sandwiched in-between two QDs, each of which couples to a cold reservoir [153–155]. Both of these designs have been experimentally implemented and shown to able to generate power [156, 157]. However, experiments remain scarce and any new experiment is always a welcome addition to the field as there is a very large discrepancy between the amount of theoretical and experimental works. New experimental devices that actually

operate as energy harvesters are particularly interesting since most experiments have historically focused on measuring α [133–137, 158–160]. Measuring the generated power can often be straight-forward, but determining the efficiency is still a very challenging task as accurate heat current measurements have only been demonstrated in a few systems under specific operating conditions [118, 161–164]. An alternative approach is to estimate the heat current using theory, which requires a very high quantitative agreement between e.g. the measured and calculated charge current to verify that the theoretical model describes the system well enough. Nevertheless, experiments determining the efficiency are important as the promise of high performance is a cornerstone of the field. Paper I takes a step in this direction by providing the first experimental efficiency estimate of a QD heat engine, verifying that it can operate at η_{CA} at maximum power and approach η_C when tuned for high efficiency. It was subsequently followed by Ref. 157 which also included an efficiency estimate, albeit at lower η, and Ref. 165 where $ZT = 35$ was observed for a device similar to the one used in paper I, but at a higher overall temperature resulting in two orbitals contributing to the transport.

8 Summary of paper I

The purpose of this study was to explore the performance limits of an experimental implementation of a QD heat engine and hopefully validate the predicted high conversion efficiency. The results show that QDs can in fact be highly efficient thermal-to-electrical steady state energy converters, a conclusion drawn from the fact that we observed $\eta \approx \eta_{CA}$ at maximum power and $\eta > 0.7\eta_C$ while still maintaining a finite output power roughly equal to half of the maximal amount.

8.1 Experimental setup

The QD used in this study was defined as a segment in a heterostructured nanowire, see Fig. 14.a, where electrons in the conduction band of the InAs nanowire were confined by InP barriers, as explained in Sec. 2.5. The ends of the nanowire were connected to an external circuit via metallic contacts deposited on top of the wire to create a SET setup. An elevated temperature of one of the reservoirs, as required to study thermoelectric effects, was created by running a current through an additional heater contact located on top of a contact for electrical biasing, separated only by a thin oxide layer for electric insulation. Furthermore, in order for the device to produce electric power a resistive load R was connected in series to the QD, see Fig. 14.b for a circuit diagram. Any current I_{th} that is thermoelectrically generated by the device then induces a bias voltage V_{QD} across the QD due to the presence of the load, and any power that is generated by the engine gets dissipated in the load $P_{th} = -I_{th} \cdot V_{QD} = I_{th}^2 \cdot R$, making a direct measurement of P_{th} possible. To get an extensive

picture of the thermoelectric performance we measured the power as V_G, R and V_{heat} (which sets the current running through the heater contact) were varied.

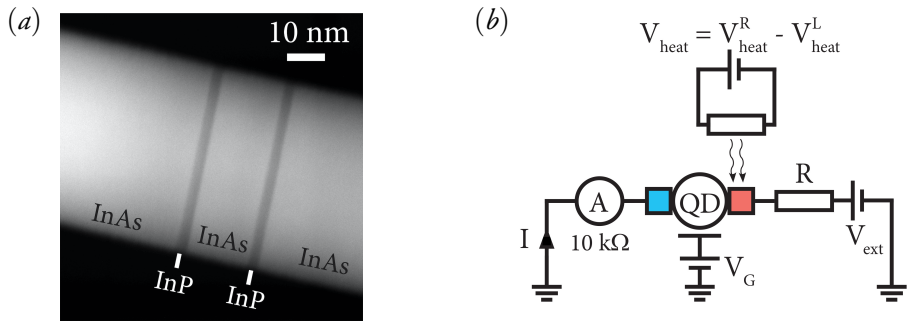

Figure 14: a) Transmission electron micrograph image of a similar QD to the one used in paper I. The electrons in the conduction band are confined between the InP barriers. b) Circuit diagram of the experimental setup where the heating circuit is electrically isolated from the QD circuit. A voltage across the heater, $|V_{heat}| > 0$, creates a temperature difference across the QD. All of the power that is thermoelectrically produced by the QD gets dissipated in the load R as long as $V_{ext} = 0$. The figure is adapted from paper I.

8.2 Analysis

The measured power allowed us to estimate the efficiency by combining P_{th} with the calculated heat current J_{Q_H} evaluated for the same values of the parameters Γ, T_H, T_C, V_G, R. This was possible since the device could be gated to a regime where its behavior was accurately described as a QD containing only a single spin-degenerate orbital with large electron-electron interactions. However, finding the perfect conditions for the experiment required performing thermoelectric measurements over large gate voltage regimes in several devices.

All performed measurements were of DC charge currents. The current was primarily measured as a function of V_G where other parameters such as V_{heat} or R were changed in between $I_{th}(V_G)$ measurements. From the current we obtained the conductance by differentiating with respect to bias voltage $G = \frac{dI}{dV_{ext}}$ at $\Delta T = 0$ and $R = 0$, and the generated power from $P_{th} = R \cdot I_{th}^2$ at $V_{ext} = 0$ V. Once the measurements were performed the steps involved in the analysis and the efficiency estimations were as follows.

1) Extract basic QD parameters from the conductance at $\Delta T = 0$. These parameters are the gate lever arm α_G and charging energy E_C, both obtained from a stability diagram, as well as Γ, which is extracted by fitting the conductance calculated using the RTD theory to the measured Coulomb peaks.

2) Extract T_H and T_C by fitting the calculated current to $I_{th}(V_G)$ measured at a finite V_{heat} and $V_{ext} = 0$, as will be discussed in section 8.3. This step was performed for each measurement of $I_{th}(V_G)$.

3) Calculate $J_{Q_H}(V_G)$ for the set of parameters extracted in steps 1-2 and combine with the measured $P_{th}(V_G)$ to obtain $\eta(V_G)$.

Unfortunately, a small signal-to-noise ratio of the current close to the theoretical maximum efficiency points gave rise to very large fluctuations of $\eta(V_G)$. We therefore chose to mainly focus on P_{th} maximized with respect to V_G, henceforth called P_{max}, and the corresponding efficiency $\eta_{P_{max}}$.

8.3 Thermometry

Due to the nanoscale size of our system, the low temperatures at which the experiment was conducted, and a non-trivial answer as to where to probe the local temperature there was no straight-forward way of measuring the temperatures of the electronic reservoirs in our setup. In order to extract information of the temperatures we therefore performed a least square fit of the current calculated using the RTD theory to the measured $I_{th}(V_G)$ with T_H and T_C as free parameters. This was done by minimizing

$$r = \sum_i (I_{experiment}(V_{G,i}) - I_{theory}(V_{G,i}))^2. \tag{79}$$

The fits acquired this way produce unique temperatures, as can be seen from an example of $r(T_H, T_C)$ in Fig. 15.a, and the agreement between the measured data and the theory is excellent, see Fig. 15b. These results, together with the fact that the analysis yielded consistent temperatures over wide ranges of V_{heat} and R, make for convincing evidence that this approach can be used as a valid thermometry tool.

It is, however, worth to mention two alternative approaches for performing thermometry in a thermally biased QD. First, an alternative way of obtaining the temperatures would be to bias the QD so that the energy level only samples the thermal distribution of one of the reservoirs [166]. However, this requires additional measurements, and the large voltage needed puts the QD outside of the regime where it can be operated as a heat engine. When instead fitting the theory to the measurements using Eq. 79 these problems are avoided. Second, it could be possible to use a normal metal-insulator-superconductor (NIS) junction to obtain the temperature of the metallic contact(s) [167], if the temperatures are low enough. This would have the benefit that it would be possible to operate the QD as a heat engine and measure the temperature at the same time. The drawback would be that the temperatures of the contacts are not necessarily the ones sought after as the reservoirs

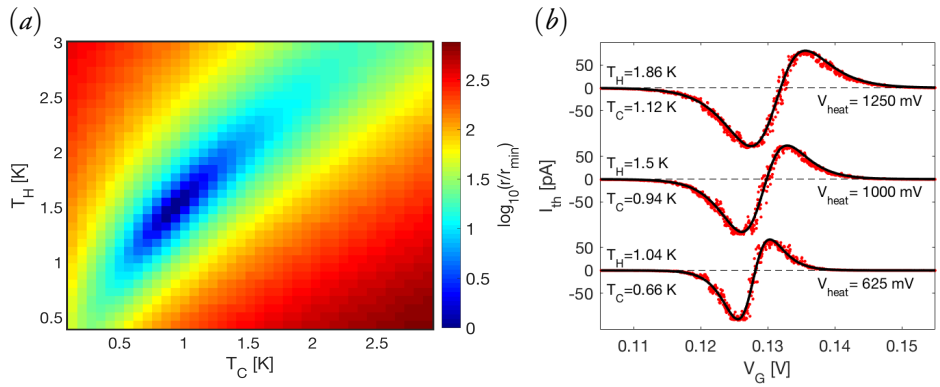

Figure 15: a) Logarithm of the summed squared residues in Eq. 79 normalized by its minimum value. Since r has one global minimum it produces a unique set of $\{T_H, T_C\}$. For this example the best fit was given by $T_H = 1.46$ K and $T_C = 0.89$ K. b) The thermometry technique yields excellent fits which is exemplified by showing three $I_{th}(V_G)$ traces measured for $R = 14.4$ kΩ. The applied V_{heat} and the resulting temperatures are indicated in the figure. The figure is adapted from paper I.

will consist of both parts of the contacts and the nanowire. Alternatively, a macroscopic metallic contact could be exchanged for a microscopic counterpart. By performing NIS thermometry on the microscale metal contact the heat flow through the QD can be directly measured [118, 164], which would be a very interesting extension to the work in paper I, albeit at the cost of needing a more complicated setup.

8.4 Results

The main results from the study are summarized in Fig. 16, which includes both experimental and theoretical data. First, it is shown how P_{max} depends on the external load R for two settings of V_{heat}, see 16.a. The power has a clear maximum for a specific value of R, around $1.0 - 1.5$ MΩ for this device, and one can also see that this value depends on the temperatures. This figure hints at the fact that it is important to optimize the load in order for the engine to show its full potential. The temperatures and thermal bias in the experiment were around $T \sim \Delta T \sim 1$ K, from which the engine can generate a few fW of electrical power.

In Fig. 16.b P_{max} is instead plotted against the corresponding efficiency $\eta_{P_{max}}$ as R is being swept. Both cases show that the efficiency at maximum power is very close to η_{CA}, confirming the theoretical predictions. Furthermore, for larger R the engine gets tuned to a point where it produces half of the maximal power, at an efficiency of $0.7\eta_C$. These results show that a QD can in fact be used as a highly efficient heat engine.

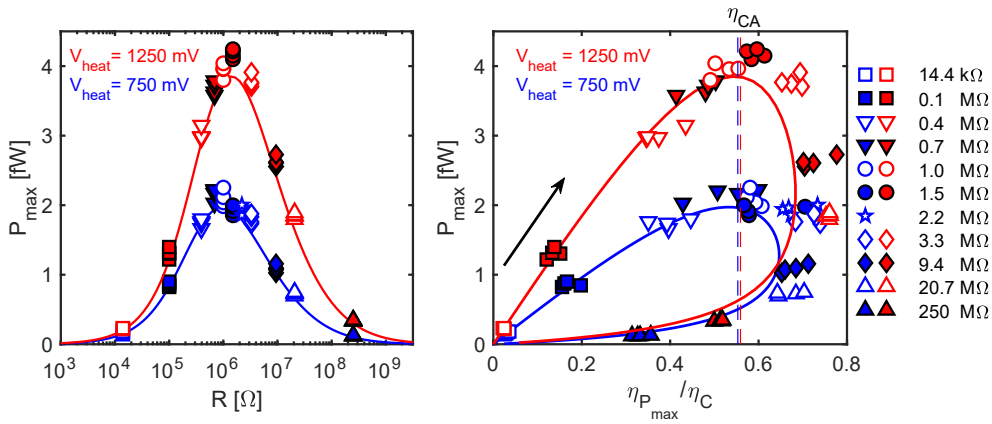

Figure 16: a) P_{max} (P_{th} maximized with respect to V_G) as a function of R shows an optimal load where the power production reaches a maximal value. The markers are measured data and the solid lines theoretical predictions. b) Parametric plot of P_{max} and the estimated $\eta_{P_{max}}$ as the load is increased. The arrow points in the direction of increasing R. The markers are based on measured P_{max} and calculated J_{Q_H}, while the solid lines are pure theoretical results. The dashed lines indicate η_{CA}, which is close to the estimated efficiency at the measured maximum power for the engine. Parameters used are $\Gamma = 8.9$ GHz and $T_C = 0.69$ K, $T_H = 1.02$ K for $V_{heat} = 750$ mV whereas $T_C = 1.13$ K, $T_H = 1.83$ K for $V_{heat} = 1250$ mV. The figure is adapted from paper I.

9 Summary of paper II

This study contains a more detailed analysis of the conditions required to optimize the power and efficiency of devices similar to the one used in paper I. The paper contains two parts. The first investigates how one best determines the load R_P that maximizes the output power. This was motivated by Fig. 16.a showing that there is a large performance penalty for choosing a sub-optimal load, and sweeping the load in order to maximize the power can be a tedious task. The analysis included both theoretical calculations using the RTD theory as well as additional power measurements on the same device that played the lead role in paper I. The second part of the study quantifies the efficiency decrease from including second order tunneling effects and how this decrease scales with the tunnel coupling. As such it provides a measure for when a sequential tunneling approach is sufficient to model a thermoelectric QD device. Both the theoretical and experimental methods are the same as in paper I and they will not be discussed further, we instead jump straight to the results.

9.1 Linear response - load matching

In electrical circuit theory any energy source with a linear IV characteristic, or network of linear components, can be modeled as a Thevenin or Norton equivalent circuit which contain only an internal resistance and an ideal voltage or current source. The ideal sources are characterized be the device's open circuit voltage and short circuit current, and the internal load by the quotient of the two. The power transferred from an energy source to an

external load is maximal when the size of the external load matches that of the internal load, a principle known as load matching. In paper II it is investigated whether such a description can be valid for the QD heat engine. This is done by comparing the load and voltage at maximum power calculated using nonlinear effects to the equivalent circuit counterparts, both obtained using the RTD theory including second order tunneling effects. The results are shown in Fig. 17 where it is evident that any differences between the two cases are very small, and the principle of load matching is, to a good approximation, valid.

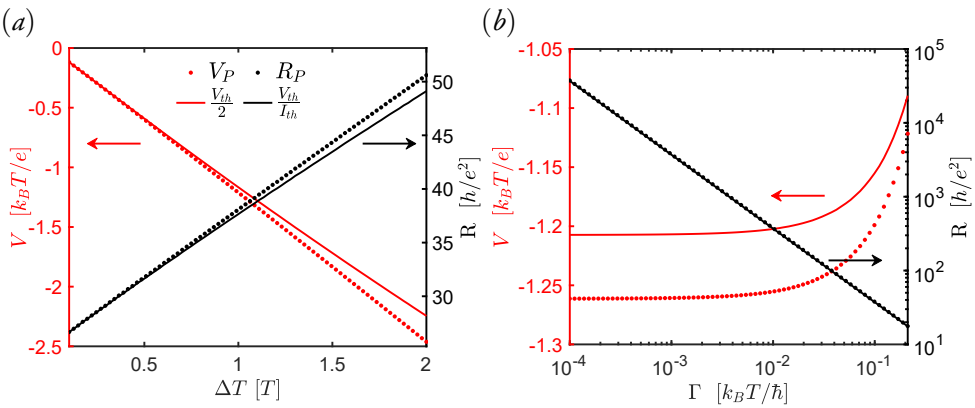

Figure 17: Comparison of the load and voltage at maximum power for a linear (solid lines) and a non-linear model (dots). The engine can in the linear regime be modeled as a Thevenin equivalent circuit with internal load V_{th}/I_{th}, for which the voltage at maximum power is half of the open circuit voltage V_{th}. Parameters used are $\hbar\Gamma = 0.1k_BT$ in (a), $\Delta T = T$ in (b) and $T = T_C$ in both figures. The figure is adapted from paper II.

9.2 Optimal load - practical considerations

The fact that load matching is approximately valid is good news for an experimentalist wanting to optimize the load. This is because the optimal load then can be obtained from the equivalent circuit's internal load $\frac{V_{th}}{I_{th}}$ evaluated at the V_G that maximizes the linear response power $\frac{1}{4}GV_{th}^2$. Here, V_{th}, I_{th} and G are the thermally induced open circuit voltage, short circuit current and conductance (for $\Delta T = 0$), respectively. An alternative approach to load matching is to experimentally determine the *effective* internal load of the device. This can be done by measuring I as a function of both V_G and V_{ext} while maintaining a thermal bias across the QD. The optimal load is then given by the value of V_{ext}/I that maximizes $-IV_{ext}$. Data generated by this approach can be seen in Fig. 18, where the predicted values for the best R coincide with those from paper I where the load was physically varied, verifying this technique. Finally, by using linear response and sequential tunneling assumptions it is possible to derive a simple expression for the optimal load

$$R_P \approx 1.25\frac{k_B(T_H + T_C)}{\hbar\Gamma}\frac{h}{e^2}, \tag{80}$$

which worked surprisingly well for the experimental device. The results from the three approaches are compared in Tab. 1, which show only minor differences between them. The best way of finding the optimal load thus comes down to the experimental tools and measurements that are available for a particular experiment.

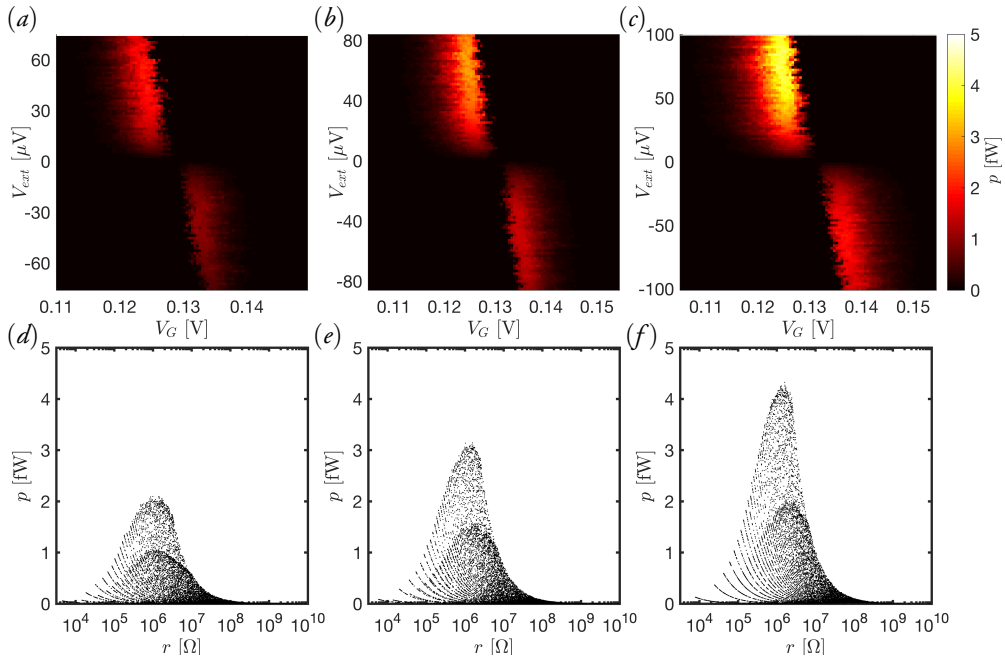

Figure 18: Power production $p = -IV_{ext}$ and effective load $r = V_{ext}/I$. (a)-(c) Experimentally measured p as a function of V_{ext} and V_G. Experimental parameters are $\Gamma = 5.8$ μeV, $U = 4.9$ meV, $\alpha = 0.05$ and $T = 0.75$ K, $\Delta T = 0.45$ K in (a), $T = 0.9$ K, $\Delta T = 0.6$ K in (b), and $T = 1.15$ K, $\Delta T = 0.7$ K in (c). Only regions where the QD produces power are shown in color. (d)-(f) Black dots show the data in (a)-(c) plotted in coordinates of p and r where each dot corresponds to the p and r for a set of $\{V_G, V_{ext}\}$. The measured r that maximizes p are roughly the same as obtained when actually varying the load and measuring power. The figure is adapted from paper II.

Table 1: Calculated optimal load for high power for the three measurements a, b and c in Fig. 18. R_P is calculated using non-linear and second order tunneling effects. V_{th}/I_{th} represent the linear response, second order tunneling results. Equation 80 is based on linear response and first order tunneling.

Measurement	R_P [MΩ]	V_{th}/I_{th} [MΩ]	Eq. 80 [MΩ]
a	0.940	0.935	0.930
b	1.157	1.150	1.144
c	1.438	1.430	1.430

9.3 Efficiency

The second part of paper II investigates how the efficiency scales with Γ when also second order tunneling effects are included, i.e. how much the effective broadening reduces the efficiency. The main results from this part can be seen in Fig. 19 where the maximum η and η at maximum power are plotted against Γ. From the figure one can see that the efficiency can only be said to approach η_C if $\hbar\Gamma$ is many orders of magnitude smaller than the thermal energy. The efficiency at maximum power is not as sensitive to increases in Γ due to the operating conditions being further away from open circuit conditions where the broadening plays a large role. Furthermore, we can see that even though we did not manage to probe the highest efficiency points for the device in paper I, we came fairly close as the maximum efficiency would be around $0.8\eta_C$ for that experiment since $20\hbar\Gamma = 2k_BT_C = k_BT_H$. The figure also includes the exact solution for the efficiency calculated for $U = 0$ as a comparison, which has been presented in earlier studies [128, 129].

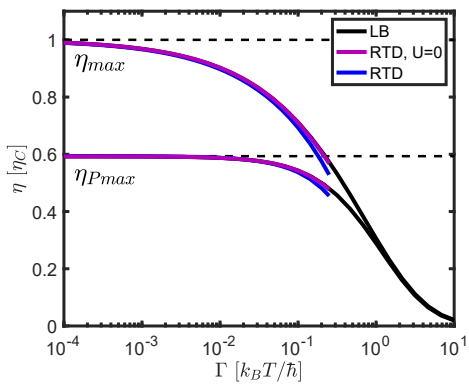

Figure 19: Maximum efficiency η_{max} and efficiency at maximum power $\eta_{P_{max}}$ as a function of Γ. Input parameters for the calculations are $\Delta T = T_C = T$ and $U = 1000k_BT$ to ensure that the doubly occupied state is unavailable for transport (blue line). Results for RTD theory with $U = 0$ (purple line) and Landauer-Büttiker transport theory (black line) are also included in the plot as references. The dashed lines indicate η_C and η_{CA}. The figure is taken from paper II.

Single bath quantum engine

Heat from a single heat bath can be converted perfectly into work if the entropy decrease of the bath is compensated for by another part of the system. This principle is exploited in this chapter where an experimentally feasible quantum engine based on coupled quantum dots is introduced and analyzed. The chapter starts with a more detailed look into the work extraction step in the Szilard engine, which is followed by an introduction to relevant parts of quantum thermodynamics. Finally, paper III, in which the double QD engine is proposed, is summarized.

10 Information and Landauer's bound

Our discovery of the intricate connection between information and thermodynamics can be dated back to Maxwell's demon and the Szilard engine introduced in Sec. 1.4. In the Szilard engine, information about a particle's position allows one to convert $k_B T \ln 2$ of heat into work at the expense of increasing the entropy of another part of the system (the demon's memory). In general, the upper bound of how much work can be extracted from a system is given by the difference in free energy of its initial and final states

$$\Delta F = \Delta U - T\Delta S. \tag{81}$$

The conundrum with the Szilard engine was that it seemed like $\Delta F = 0$ even though work was extracted. A proposed solution to this contradiction is to consider the demon's memory to be part of the system, which ensures $\Delta F \neq 0$. In paper III an engine with close similarities to the Szilard engine is proposed, and in order to understand its operation it is illustrative to analyze the free energy change of the work extraction step in the Szilard engine (ignoring the memory). When evaluating ΔF we can consider the particle to be in one of two well-defined states: in the left or right half of the compartment. The occupation probabilities for the two states will be denoted p_L and p_R. Work extraction begins after the demon observes the particle's state, e.g. $p_L = 1$ and $p_R = 0$, which results in complete certainty of the particle's position and thus $S = 0$ according to Eq. 10. After work has been

extracted we no longer know where the particle is, and it must be considered to have equal probabilities of being in both states. In that case $p_L = p_R = \frac{1}{2}$, for which $S = k_B \ln 2$. The total difference in internal energy is $\Delta U = 0$ since Szilard considered an ideal gas where U only depends on the number of particles and T, which do not change. Thus, we end up with $\Delta F = -k_B T \ln 2$ where a decrease in F indicates that the process is spontaneous, allowing us to extract work.

The process just described is the inverse of a Landauer erasure [20]. Landauer's principle states that the minimum average energy required to erase an arbitrary bit of information is $k_B T \ln 2$. In that case one considers the initial state to be the most general state where the physical system encoding the information has equal probabilities of being in both the 0 and 1 state (in the Szilard engine this is given by $p_L = p_R = \frac{1}{2}$). The final state is a predetermined state of the bit, e.g. 0 ($p_R = 0$). Hence, an empty memory is represented as a string of 0s, which is a well-defined state with zero entropy. An empty memory can thus be used as an entropy sink making it possible to use it as a resource [168, 169]. The beauty of Landauer's principle, and its inverse, is that it is completely system agnostic, and the dissipation limit for memory erasure has recently been experimentally verified by very delicate measurements in different systems [170–175]. Alternative versions of the principle have been identified where the resource spent is not in the form of energy, but rather some other quantity such as angular momentum [176, 177]. Common for all approaches is, however, that the resource needed is determined by the entropy (information) change of the system.

The link between information and thermodynamics, especially in small systems with few degrees of freedom, is being studied extensively today and there is a plethora of suggestions of different systems with Maxwell's demon-like abilities. There are also experiments probing the concept of using information to convert heat from a single heat bath into work. Most notable are several experimental implementations of electronic engines acting as information driven generators and coolers [172, 178–183]. Engines utilizing electrons are particularly interesting as they can potentially be incorporated into electronic circuits.

11 Quantum thermodynamics

Up until this, nearly final, section only classical thermodynamics has been required to analyze the various systems. It remains a perfectly valid tool as long as the possible microstates of a system are well defined pure states and fluctuations remain small compared to average quantities. However, the picture can be quite different when the system under consideration exhibit strong quantum properties such as quantum coherence and correlations. The classical definitions of the thermodynamic quantities are not always valid in these cases and

the problem needs to treated within the framework of quantum thermodynamics (QTD). The research field of QTD is extraordinarily active at the moment and a comprehensive overview of it is well beyond the scope of this thesis. A curious reader is instead encouraged to consult Refs. 184 and 185. One of the big open questions in QTD is how to approach unified definitions of work and heat in quantum systems. There are currently several definitions, sometimes valid for different systems in different regimes, but no general and unambiguous definition exists [184]. For our purposes only ensemble averages are of interest for which work and heat can be defined as (assuming weak system-bath coupling) [186]

$$W = \int_{t_o}^{t_{final}} \mathrm{Tr}\left[\frac{dH(t)}{dt}\rho(t)\right] dt, \tag{82}$$

$$Q = \int_{t_o}^{t_{final}} \mathrm{Tr}\left[H(t)\frac{d\rho(t)}{dt}\right] dt, \tag{83}$$

where $H(t)$ is the system's Hamiltonian and $\rho(t)$ its density matrix. This definition is consistent with the first law of (classical) thermodynamics.

One branch of QTD focuses on studying how to create machines that are driven by (see e.g. Refs. 187–190), or generate [191], quantum resources making them true quantum engines. Ideally one wants the quantum engine to outperform its classical counterpart, however the bounds set by classical thermodynamics, such as η_C and Landauer's bound remain valid also in the quantum regime. The latter has even been experimentally verified [192, 193]. However, there is in general a lack of experiments in the field, both when it comes to testing fundamental principles and creating quantum engines, and it would thus benefit greatly from any new experiment. This is where paper III aims at making a contribution by proposing an experimentally feasible quantum engine.

12 Summary of paper III

In paper III we propose a quantum engine that extracts work from a single heat bath by letting initial, entangled, states act as the entropy sink. The final state of the cycle has the same energy as the initial state, just like in the Szilard engine, but will be a mixed thermal state instead of a pure entangled state. Since the entanglement is destroyed in the process we use the terminology that it acts as the engine's fuel.

The physical system we have in mind for the proposed engine consists of two electrons on a double QD. Double QD systems are commonly studied in research environments, mostly for their interesting transport and spin properties. For example, they can be used to create qubits where information is encoded in the entangled spin states of two electrons [53, 55, 194], which happen to be the same states that our engine is based on. Qubits

based on spins in QDs is an experimentally mature technology and an implementation of the proposed engine should thus be fairly straight forward and possible in the near future.

12.1 Double quantum dot

A schematic of the double QD system studied in paper III is shown in Fig. 20.a where two plunger gates can be used to individually tune the potential energies of electrons on the QDs. A third gate is used to control the tunnel coupling λ between the QDs. Electrons in the system interact with one another through Coulomb interactions on the same and different QDs with strengths U and U_{LR}, respectively. One spin-degenerate orbital per QD is included, which results in a six-dimensional Hilbert space for the two-electron states. Energetically, two of the states will be split off from the remaining four by $\sim U$, which we take to be very large ($U \gg k_B T$). For simplicity we also set the single particle energies to $\varepsilon_1 = \varepsilon_2 = 0$ as well as $U_{LR} = 0$.

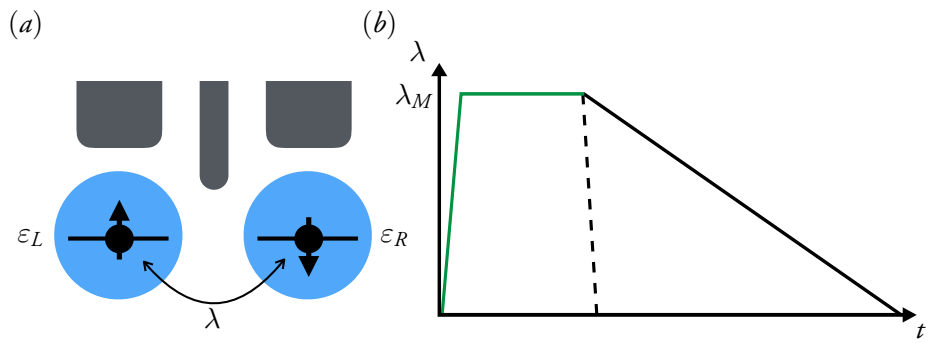

Figure 20: a) Schematic of a double QD where plunger gates (gray) control the single particle energies ε of each QD, as well as the inter-QD tunnel coupling λ. b) Tunnel coupling λ as a function of time for both cycles. The green lines indicate the parts common for both cycles, the dashed black line represents cycle (i) and the solid black line cycle (ii). (a) is adapted from paper III.

When $\lambda = 0$ the four lowest energy eigenstates, all at $E = 0$, can be written

$$|S_0\rangle = \frac{1}{\sqrt{2}}\left(c^\dagger_{1\uparrow}c^\dagger_{2\downarrow} - c^\dagger_{1\downarrow}c^\dagger_{2\uparrow}\right)|0\rangle, \quad |T_+\rangle = c^\dagger_{1\uparrow}c^\dagger_{2\uparrow}|0\rangle, \tag{84}$$

$$|T_0\rangle = \frac{1}{\sqrt{2}}\left(c^\dagger_{1\uparrow}c^\dagger_{2\downarrow} + c^\dagger_{1\downarrow}c^\dagger_{2\uparrow}\right)|0\rangle, \quad |T_-\rangle = c^\dagger_{1\downarrow}c^\dagger_{2\downarrow}|0\rangle, \tag{85}$$

where S and T denote whether the spin-state is a singlet or a triplet. When λ is increased all Ts remain eigenstates, but $|S_o\rangle$ gets mixed with the high energy state $|S_+\rangle =$

$\frac{1}{\sqrt{2}}\left(c^\dagger_{1\uparrow}c^\dagger_{1\downarrow}+c^\dagger_{2\uparrow}c^\dagger_{2\downarrow}\right)$ to form

$$|S_m\rangle = \frac{1}{\sqrt{E_{S_m}^2+4\lambda^2}}\left(2\lambda|S_0\rangle + E_{S_m}|S_+\rangle\right). \tag{86}$$

The energy of the triplets is still $E_T(\lambda)=0$ whereas the mixed singlet's energy is

$$E_{S_m}(\lambda) = \frac{U}{2} - \sqrt{\frac{U^2}{4}+4\lambda^2} < 0. \tag{87}$$

This energy spectrum and its dependency on λ constitutes the basis of the engine.

12.2 Engine operation

We consider two cycles for work extraction, both relying on only changing λ, albeit in different manners as is shown in Fig. 20.b. Both cycles start with the electrons in the state $|S_0\rangle$ at $\lambda = 0$. The $|S_0\rangle$ state is assumed to be provided by some external entity, e.g. as a left-over from a computation or simulation in future quantum computers. In the next step λ is quickly increased to large value λ_M. This step needs to be fast enough to inhibit heat exchange with the environment (i.e. thermodynamically adiabatic), but slow enough that the system remains in $|S_m\rangle$ (i.e. quantum mechanically adiabatic). Since this changes the energy spectrum, i.e. the Hamiltonian, but not the occupation probabilities, i.e. the density matrix, work is being extracted from the system in accordance with Eq. 82. Next one waits at $\lambda = \lambda_M$ for a long time such that the system relaxes and the electrons end up in thermal equilibrium with their environment, which is treated as a heat bath. The occupation probabilities for the different states is then given by the Boltzmann distribution in Eq. 9. Since the relaxation does not change the Hamiltonian but only reshuffles the probabilities this step corresponds to absorbing heat from the heat bath, see Eq. 83. For the final step the two cycles differ. In the first cycle, called (i), λ is quickly decreased to $\lambda = 0$ in order to avoid further interactions between the electrons and the bath. In (ii) λ is instead decreased very slowly such that the process is isothermal (and hence quasistatic). The energy changes during these final steps are associated with both work and heat.

12.3 Performance

When evaluating the total work output for the (ideal) cycles one obtains

$$W^{(i)} = -\frac{3}{Z}\delta E, \tag{88}$$

$$W^{(ii)} = -\delta E - k_B T\left(\ln 4 - \ln Z\right), \tag{89}$$

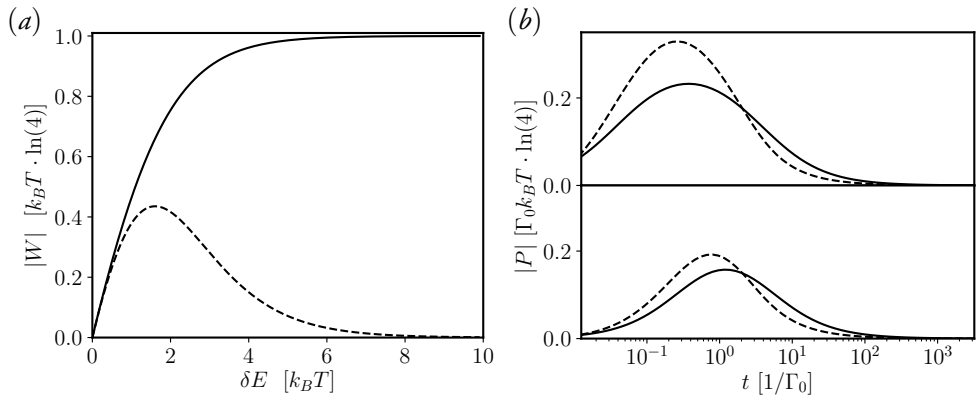

Figure 21: a) Work output for cycle (i), dashed line, and cycle (ii), solid line, as a function of the singlet-triplet energy split δE at λ_M. Cycle (ii) provides the largest work output, which is equal to ΔF for large δE. b) Power output as a function of cycle time for the two cycles (same labels as in (a)) when finite time effects are included. Time is given in units of $1/\Gamma_0$ where $\Gamma_0 = \gamma\nu_0/k_BT$ corresponds to the transition time between (almost) degenerate states when the double QD is coupled to a phonon bath with linear dispersion $\nu(\varepsilon_k) = \nu_0\varepsilon_k$. An initialization time t_{init} for the qubits is included when calculating power. t_{init} is $0.04\Gamma_0^{-1}$ in the top figure and $0.4\Gamma_0^{-1}$ in the bottom one. The figure is adapted from paper III.

where $\delta E = E_T(\lambda_M) - E_S(\lambda_M)$ and $Z = 3 + \exp(\delta E/k_BT)$ denotes the partition function. How the output work per cycle depends on δE is shown in Fig. 21.a where it is clear that cycle (ii) always generates more work than cycle (i). In the limit of large δE the engine is thermodynamically ideal when using cycle (ii) as the work output equals ΔF, which in this case is $-k_BT\ln 4$ due to the four possible final states and the fact that $\Delta U = 0$.

Paper III also includes an analysis of the engine including finite-time effects. These are taken into account by including a microscopic description of a phononic heat bath and an explicit system-bath coupling of the form

$$H_B = \sum_{\omega} \varepsilon_k b_k^\dagger b_k + \sum_{i,k} \gamma c_{i,\sigma}^\dagger c_{i,\bar{\sigma}} (b_k^\dagger + b_k) + h.c., \tag{90}$$

where interactions with some magnetic environment are assumed to cause spin-flips of the individual electrons. The energy required to transition between the different states is supplied, or absorbed, by the phonon bath. In Eq. 90 b_k is a boson field operator for mode k, γ is the system-bath coupling strength and c a fermion field operator. The system's dynamics is calculated by solving the time-dependent Lindblad master equation in Eq. 71 using $|S_0\rangle$ as the initial state. This provides the density matrix $\rho(t)$, which together with the double QD Hamiltonian is used to evaluate the work in Eq. 82.

The power output of the engine is shown in Fig. 21.b where it is evident that the two cycles have different regimes where they are advantageous. As a rule of thumb cycle (ii) is preferable is when the cycle time is longer than the relaxation time of almost degenerate states, i.e. the relaxation time of the initial state, otherwise cycle (i) is better.

Outlook

These are exiting times for everyone interested in nanoscale heat engines and quantum thermodynamics. We, as in the research community, are at a place where technological advancements will make many novel experiments possible in the near future, and theoretical breakthroughs will most certainly increase our understanding of heat and work in the quantum realm. We will thus – hopefully – see working implementations of both new and existing engine designs rather soon. These will be both nanoscale heat engines driven as generators or coolers, as well as truly quantum engines. The scientific contributions discussed in this thesis all aim at increasing our understanding of QD-based heat engines as well as lowering the bar for performing new experiments.

Specifically, the results of the studies in papers I and II verify that QDs can be used as the central components in highly efficient solid-state heat engines, and shine light on how to best operate such engines. These are very timely contributions as the large body of theoretical research on different QD heat engines often rely on the fact that QDs are perfect energy filters and that engines based on them are optimal thermodynamic engines. We now know that this is a fairly good approximation in many, but not all, cases. In contrast to the devices studied in this thesis most of the future experimental implementations will probably have a more complicated design than a single QD in a SET setup. However, they will all use QDs as the minimal component allowing a high efficiency, and the results presented here remain valid also for those cases. Regarding practical usefulness of the devices it is unlikely that QDs will be used as energy filters in room temperature energy harvesters. This is due to their small level spacings and interaction energies compared to the thermal energy, which drastically lowers the efficiency. However, it is possible that other QD-like systems with more favorable energy scales could be useful, for which the results in this thesis would also be applicable. An example is single molecules, which have both large interaction energies and level spacings, and where quantum interference effects can further boost the thermoelectric performance [195]. It is also possible that QD devices will be used as refrigerators spot-cooling electronic or quantum circuits at cryogenic temperatures where these issues are not present.

A subtler lesson from papers I and II, at least for the authors, is that when conducting studies like these good performance can require a tight coupling also between theoretical and experimental scientists. We are currently at a point where a high degree of control of experimental devices and advanced theoretical methods allow for quantitative comparisons to be used as a probe of otherwise inaccessible parameters. In general, this requires flexibility and diverse toolboxes from both parties. From a broader scientific view new results are of course more robust if the analyses of the experiments can be free from theoretical assumptions, but where the observed data can later be fully explained even using said assumptions. However, results derived from a combination of theory and experiment can be ever so important when the experiments are limited by present-day technology.

Paper III did not verify or optimize the performance of an existing device but instead proposed a completely new type of engine and experiment. It is unknown whether the experiment will ever be conducted, but it nevertheless contributes to the field as there is currently a lack of even theoretical propositions of quantum engines that are feasible with current technologies. On the other hand, it is not unreasonable to argue that engines similar to this one can be practically useful, especially in future quantum computers where specific quantum (entangled) states may be abundant and can thus be used as a resource. Exactly how the engines would work in that case will depend on several things, e.g. the implementation of a qubit, but the physical principles used in paper III can be used also for systems not based on QDs.

References

[1] S. Carnot. *Réflexions sur la puissance motrice du feu et sur les machines propres a développer cette puissance*. Bachelier, 1824.

[2] R. Clausius. Über verschiedene für die anwendung bequeme formen der hauptgleichungen der mechanischen wärmetheorie. *Annalen der Physik*, 201(7):353–400, 1865.

[3] D. Kondepudi and I. Prigogine. *Modern thermodynamics: from heat engines to dissipative structures*. John Wiley & Sons, 2014.

[4] D. Chandler. Introduction to modern statistical mechanics. *Oxford University Press, Oxford, UK*, 1987.

[5] A. E. Allahverdyan, K. V. Hovhannisyan, A. V. Melkikh, and S. G. Gevorkian. Carnot cycle at finite power: attainability of maximal efficiency. *Physical Review Letters*, 111(5):050601, 2013.

[6] M. Campisi and R. Fazio. The power of a critical heat engine. *Nature communications*, 7(1):1–5, 2016.

[7] N. Shiraishi, K. Saito, and H. Tasaki. Universal trade-off relation between power and efficiency for heat engines. *Physical Review Letters*, 117(19):190601, 2016.

[8] C. Van den Broeck. Thermodynamic efficiency at maximum power. *Physical Review Letters*, 95(19):190602, 2005.

[9] I. I. Novikov. The efficiency of atomic power stations (a review). *Journal of Nuclear Energy (1954)*, 7(1-2):125–128, 1958.

[10] P. Chambadal. Las centrales nucleares. 4:1–58, 1957.

[11] F. L. Curzon and B. Ahlborn. Efficiency of a carnot engine at maximum power output. *American Journal of Physics*, 43(1):22–24, 1975.

[12] M. Esposito, R. Kawai, K. Lindenberg, and C. Van den Broeck. Efficiency at maximum power of low-dissipation carnot engines. *Physical Review Letters*, 105(15):150603, 2010.

[13] M. Esposito, K. Lindenberg, and C. Van den Broeck. Thermoelectric efficiency at maximum power in a quantum dot. *EPL (Europhysics Letters)*, 85(6):60010, 2009.

[14] M. Esposito, K. Lindenberg, and C. Van den Broeck. Universality of efficiency at maximum power. *Physical Review Letters*, 102(13):130602, 2009.

[15] P. A. Jacquet. Thermoelectric transport properties of a chain of quantum dots with self-consistent reservoirs. *Journal of Statistical Physics*, 134(4):709–748, 2009.

[16] J. Meair, J. P. Bergfield, C. A. Stafford, and P. Jacquod. Local temperature of out-of-equilibrium quantum electron systems. *Physical Review B*, 90(3):035407, 2014.

[17] J. C. Maxwell. *Theory of heat*. Longmans, Green, 1891.

[18] L. Szilard. Über die entropieverminderung in einem thermodynamischen system bei eingriffen intelligenter wesen. *Zeitschrift für Physik*, 53(11-12):840–856, 1929.

[19] L. Brillouin. The negentropy principle of information. *Journal of Applied Physics*, 24(9):1152–1163, 1953.

[20] R. Landauer. Irreversibility and heat generation in the computing process. *IBM Journal of Research and Development*, 5(3):183–191, July 1961.

[21] C. H. Bennett. The thermodynamics of computation—a review. *International Journal of Theoretical Physics*, 21(12):905–940, 1982.

[22] C. H. Bennett. Demons, engines and the second law. *Scientific American*, 257(5):108–117, 1987.

[23] L. De Broglie. *Recherches sur la théorie des quanta*. PhD thesis, Migration-université en cours d'affectation, 1924.

[24] E. Schrödinger. Quantisierung als eigenwertproblem. *Annalen der physik*, 385(13):437–490, 1926.

[25] J. J. Sakurai, J. Napolitano, et al. *Modern quantum mechanics*, volume 185. Pearson Harlow, 2014.

[26] R. M. Martin. *Electronic Structure. Basic Theory and Practical Methods.* Cambridge University Press, 2012.

[27] D. R. Hartree. The wave mechanics of an atom with a non-coulomb central field. part i, ii and iii. theory and methods. In *Mathematical Proceedings of the Cambridge Philosophical Society*, volume 24, pages 89–110. Cambridge University Press, 1928.

[28] F. Bloch. Über die quantenmechanik der elektronen in kristallgittern. *Zeitschrift für physik*, 52(7-8):555–600, 1929.

[29] H. Ibach and H. Lüth. An introduction to principles of materials science. *Solid State and Physics, Springer, Berlin*, page 244, 1995.

[30] J. D. Patterson and B. C. Bailey. *Solid-state physics: introduction to the theory*. Springer Science & Business Media, 2007.

[31] M. Dresselhaus, G. Dresselhaus, S. B. Cronin, and A. G. Souza Filho. *Solid State Properties*. Springer, 2018.

[32] G. H. Wannier. The structure of electronic excitation levels in insulating crystals. *Physical Review*, 52(3):191, 1937.

[33] J. C. Slater. Electrons in perturbed periodic lattices. *Physical Review*, 76(11):1592, 1949.

[34] J. H. Davies. *The physics of low-dimensional semiconductors: an introduction*. Cambridge university press, 1998.

[35] M. G. Burt. The justification for applying the effective-mass approximation to microstructures. *Journal of Physics: Condensed Matter*, 4(32):6651, 1992.

[36] H. L. Störmer, R. Dingle, A. C. Gossard, W. Wiegmann, and M. D. Sturge. Two-dimensional electron gas at a semiconductor-semiconductor interface. *Solid state communications*, 29(10):705–709, 1979.

[37] H. Y. Hwang, Y. Iwasa, M. Kawasaki, B. Keimer, N. Nagaosa, and Y. Tokura. Emergent phenomena at oxide interfaces. *Nature materials*, 11(2):103–113, 2012.

[38] J.-P. Colinge, X. Baie, V. Bayot, and E. Grivei. A silicon-on-insulator quantum wire. *Solid-State Electronics*, 39(1):49–51, 1996.

[39] A. Jorio, G. Dresselhaus, and M. S. Dresselhaus. *Carbon nanotubes: advanced topics in the synthesis, structure, properties and applications*, volume 111. Springer Science & Business Media, 2007.

[40] R. S. Wagner and W. C. Ellis. Vapor-liquid-solid mechanism of single crystal growth. *Applied physics letters*, 4(5):89–90, 1964.

[41] K. Hiruma, M. Yazawa, T. Katsuyama, K. Ogawa, K. Haraguchi, M. Koguchi, and H. Kakibayashi. Growth and optical properties of nanometer-scale gaas and inas whiskers. *Journal of Applied Physics*, 77(2):447–462, 1995.

[42] B. J. Van Wees, H. Van Houten, C. W. J. Beenakker, J. G. Williamson, L. P. Kouwenhoven, D. Van der Marel, and C. T. Foxon. Quantized conductance of point contacts in a two-dimensional electron gas. *Physical Review Letters*, 60(9):848, 1988.

[43] U. Meirav, M. A. Kastner, and S. Wind. Single-electron charging and periodic conductance resonances in gaas nanostructures. *Physical Review Letters*, 65(6):771, 1990.

[44] A. T. Johnson, L. P. Kouwenhoven, W. De Jong, N. C. Van der Vaart, C. J. P. M. Harmans, and C. T. Foxon. Zero-dimensional states and single electron charging in quantum dots. *Physical Review Letters*, 69(10):1592, 1992.

[45] C. Fasth, A. Fuhrer, M. T. Björk, and L. Samuelson. Tunable double quantum dots in inas nanowires defined by local gate electrodes. *Nano Letters*, 5(7):1487–1490, 2005.

[46] C. Thelander, T. Mårtensson, M. T. Björk, B. J. Ohlsson, M. W. Larsson, L. R. Wallenberg, and L. Samuelson. Single-electron transistors in heterostructure nanowires. *Applied Physics Letters*, 83(10):2052–2054, 2003.

[47] K. A. Dick, C. Thelander, L. Samuelson, and P. Caroff. Crystal phase engineering in single inas nanowires. *Nano Letters*, 10(9):3494–3499, 2010.

[48] M. Nilsson, L. Namazi, S. Lehmann, M. Leijnse, K. A. Dick, and C. Thelander. Single-electron transport in inas nanowire quantum dots formed by crystal phase engineering. *Physical Review B*, 93(19):195422, 2016.

[49] U. Resch-Genger, M. Grabolle, S. Cavaliere-Jaricot, R. Nitschke, and T. Nann. Quantum dots versus organic dyes as fluorescent labels. *Nature methods*, 5(9):763, 2008.

[50] W. C. W. Chan and S. Nie. Quantum dot bioconjugates for ultrasensitive nonisotopic detection. *Science*, 281(5385):2016–2018, 1998.

[51] T.-H. Kim, K.-S. Cho, E. K. Lee, S. J. Lee, J. Chae, J. W. Kim, D. H. Kim, J.-Y. Kwon, G. Amaratunga, S. Y. Lee, et al. Full-colour quantum dot displays fabricated by transfer printing. *Nature photonics*, 5(3):176–182, 2011.

[52] Y. Shirasaki, G. J. Supran, M. G. Bawendi, and V. Bulović. Emergence of colloidal quantum-dot light-emitting technologies. *Nature Photonics*, 7(1):13, 2013.

[53] D. Loss and D. P. DiVincenzo. Quantum computation with quantum dots. *Physical Review A*, 57(1):120, 1998.

[54] B. Trauzettel, D. V. Bulaev, D. Loss, and G. Burkard. Spin qubits in graphene quantum dots. *Nature Physics*, 3(3):192–196, 2007.

[55] R. Hanson, L. P. Kouwenhoven, J. R. Petta, S. Tarucha, and L. M. K. Vandersypen. Spins in few-electron quantum dots. *Reviews of modern physics*, 79(4):1217, 2007.

[56] M. D. Shulman, O. E. Dial, S. P. Harvey, H. Bluhm, V. Umansky, and A. Yacoby. Demonstration of entanglement of electrostatically coupled singlet-triplet qubits. *Science*, 336(6078):202–205, 2012.

[57] C. Kloeffel and D. Loss. Prospects for spin-based quantum computing in quantum dots. *Annual Review of Condensed Matter Physics*, 4(1):51–81, 2013.

[58] T. A. Fulton and G. J. Dolan. Observation of single-electron charging effects in small tunnel junctions. *Physical Review Letters*, 59(1):109, 1987.

[59] L. P. Kouwenhoven, N. C. Van der Vaart, A. T. Johnson, W. Kool, C. J. P. M. Harmans, J. G. Williamson, A. A. M. Staring, and C. T. Foxon. Single electron charging effects in semiconductor quantum dots. *Zeitschrift für Physik B Condensed Matter*, 85(3):367–373, 1991.

[60] C. W. J. Beenakker and A. A. M. Staring. Theory of the thermopower of a quantum dot. *Physical Review B*, 46(15):9667, 1992.

[61] L. P. Kouwenhoven, C. M. Marcus, P. L. McEuen, S. Tarucha, R. M. Westervelt, and N. S. Wingreen. Electron transport in quantum dots. In *Mesoscopic electron transport*, pages 105–214. Springer, 1997.

[62] M. Nilsson. *Charge and Spin Transport in Parallel-Coupled Quantum Dots in Nanowires*. Division of Solid State Physics, Department of Physics, Lund University, 2018.

[63] E. Bonet, M. M. Deshmukh, and D. C. Ralph. Solving rate equations for electron tunneling via discrete quantum states. *Physical Review B*, 65(4):045317, 2002.

[64] R. Landauer. Spatial variation of currents and fields due to localized scatterers in metallic conduction. *IBM Journal of research and development*, 1(3):223–231, 1957.

[65] M. Büttiker. Four-terminal phase-coherent conductance. *Physical Review Letters*, 57(14):1761, 1986.

[66] Y. Meir and N. S. Wingreen. Landauer formula for the current through an interacting electron region. *Physical Review Letters*, 68(16):2512, 1992.

[67] A.-P. Jauho, N. S. Wingreen, and Y. Meir. Time-dependent transport in interacting and noninteracting resonant-tunneling systems. *Physical Review B*, 50(8):5528, 1994.

[68] T. A. Costi, A. C. Hewson, and V. Zlatic. Transport coefficients of the anderson model via the numerical renormalization group. *Journal of Physics: Condensed Matter*, 6(13):2519, 1994.

[69] C. Timm. Tunneling through molecules and quantum dots: Master-equation approaches. *Physical Review B*, 77(19):195416, 2008.

[70] S. Koller, M. Grifoni, M. Leijnse, and M. R. Wegewijs. Density-operator approaches to transport through interacting quantum dots: Simplifications in fourth-order perturbation theory. *Physical Review B*, 82(23):235307, 2010.

[71] H. Schoeller and G. Schön. Resonant tunneling and charge fluctuations in mesoscopic tunnel junctions. *Physica B: Condensed Matter*, 203(3-4):423–431, 1994.

[72] H. Schoeller and G. Schön. Mesoscopic quantum transport: Resonant tunneling in the presence of a strong coulomb interaction. *Physical Review B*, 50(24):18436, 1994.

[73] J. König, H. Schoeller, and G. Schön. Resonant tunneling and coulomb oscillations. *EPL (Europhysics Letters)*, 31(1):31, 1995.

[74] M. Leijnse and M. R. Wegewijs. Kinetic equations for transport through single-molecule transistors. *Physical Review B*, 78(23):1–16, 2008.

[75] H. Schoeller. A perturbative nonequilibrium renormalization group method for dissipative quantum mechanics. *The European Physical Journal Special Topics*, 168(1):179–266, 2009.

[76] R. B. Saptsov and M. R. Wegewijs. Fermionic superoperators for zero-temperature nonlinear transport: Real-time perturbation theory and renormalization group for Anderson quantum dots. *Physical Review B*, 86(23), 2012.

[77] R. B. Saptsov and M. R. Wegewijs. Time-dependent quantum transport: Causal superfermions, exact fermion-parity protected decay modes, and Pauli exclusion principle for mixed quantum states. *Physical Review B*, 90(4), 2014.

[78] M. Governale, M. G. Pala, and J. König. Real-time diagrammatic approach to transport through interacting quantum dots with normal and superconducting leads. *Physical Review B*, 77(13):134513, 2008.

[79] M. Misiorny, M. Hell, and M. R. Wegewijs. Spintronic magnetic anisotropy. *Nature Physics*, 9(12):801–805, 2013.

[80] M. Hell, B. Sothmann, M. Leijnse, M. R. Wegewijs, and J. König. Spin resonance without spin splitting. *Physical Review B*, 91(19):195404, 2015.

[81] N. M. Gergs, S. A. Bender, R. A. Duine, and D. Schuricht. Spin Switching via Quantum Dot Spin Valves. *Physical Review Letters*, 120(1), 2018.

[82] N. M. Gergs, C. B. M. Hörig, M. R. Wegewijs, and D. Schuricht. Charge fluctuations in nonlinear heat transport. *Physical Review B*, 91(20):201107, 2015.

[83] N. M. Gergs. *Transport and topological states in strongly correlated nanostructures*. PhD thesis, Utrecht University, 2017.

[84] M. Pletyukhov and H. Schoeller. Nonequilibrium kondo model: Crossover from weak to strong coupling. *Physical Review Letters*, 108(26):260601, 2012.

[85] N. W. Talarico, S. Maniscalco, and N. L. Gullo. Study of the energy variation in many-body open quantum systems: Role of interactions in the weak and strong coupling regimes. *Physical Review B*, 101(4):045103, 2020.

[86] M. F. Ludovico, J. S. Lim, M. Moskalets, L. Arrachea, and D. Sánchez. Dynamical energy transfer in ac-driven quantum systems. *Physical Review B*, 89(16):161306, 2014.

[87] N. M. Gergs, R. Saptsov, M. R. Wegewijs, and D. Schuricht. Unpublished.

[88] V. Gorini, A. Kossakowski, and E. C. G. Sudarshan. Completely positive dynamical semigroups of n-level systems. *Journal of Mathematical Physics*, 17(5):821–825, 1976.

[89] G. Lindblad. On the generators of quantum dynamical semigroups. *Communications in Mathematical Physics*, 48(2):119–130, 1976.

[90] A. Rivas, A. D. K. Plato, S. F. Huelga, and M. B. Plenio. Markovian master equations: a critical study. *New Journal of Physics*, 12(11):113032, 2010.

[91] T. E. Humphrey and H. Linke. Quantum, cyclic, and particle-exchange heat engines. *Physica E: Low-dimensional Systems and Nanostructures*, 29(1-2):390–398, 2005.

[92] T. E. Humphrey, R. Newbury, R. P. Taylor, and H. Linke. Reversible quantum brownian heat engines for electrons. *Physical Review Letters*, 89(11):116801, 2002.

[93] T. E. Humphrey and H. Linke. Reversible thermoelectric nanomaterials. *Physical Review Letters*, 94(9):096601, 2005.

[94] O. Kedem and S. R. Caplan. Degree of coupling and its relation to efficiency of energy conversion. *Transactions of the Faraday Society*, 61:1897–1911, 1965.

[95] L. I. Anatychuk. On the discovery of thermoelectricity by volta. *Journal of Thermoelectricity*, (2):5–10, 2004.

[96] T. J. Seebeck. Ueber die magnetische polarisation der metalle und erze durch temperaturdifferenz. *Annalen der Physik*, 82(3):253–286, 1826.

[97] J. C. Peltier. Nouvelles expériences sur la caloricité des courants électrique. *Annales de chimie et de physique*, 56(371):371–386, 1834.

[98] W. Thomson. 4. on a mechanical theory of thermo-electric currents. *Proceedings of the Royal society of Edinburgh*, 3:91–98, 1857.

[99] G. Benenti, G. Casati, K. Saito, and R. S. Whitney. Fundamental aspects of steady-state conversion of heat to work at the nanoscale. *Physics Reports*, 694:1–124, 2017.

[100] B. Muralidharan and M. Grifoni. Performance analysis of an interacting quantum dot thermoelectric setup. *Physical Review B*, 85(15):155423, 2012.

[101] J. Meair and P. Jacquod. Scattering theory of nonlinear thermoelectricity in quantum coherent conductors. *Journal of Physics: Condensed Matter*, 25(8):082201, 2013.

[102] R. S. Whitney. Nonlinear thermoelectricity in point contacts at pinch off: A catastrophe aids cooling. *Physical Review B*, 88(6):064302, 2013.

[103] G. V. Chester and A. Thellung. The law of wiedemann and franz. *Proceedings of the Physical Society*, 77(5):1005, 1961.

[104] J. Goldsmid. *The physics of thermoelectric energy conversion*. Morgan & Claypool Publishers, 2017.

[105] A. F. Ioffe. *Semiconductor thermoelements and thermoelectric cooling*. Infosearch, 1957.

[106] L. E. Bell. Cooling, heating, generating power, and recovering waste heat with thermoelectric systems. *Science*, 321(5895):1457–1461, 2008.

[107] B. Yang, H. Ahuja, and T. N. Tran. Thermoelectric technology assessment: application to air conditioning and refrigeration. *HVAc&R Research*, 14(5):635–653, 2008.

[108] G. J. Snyder and E. S. Toberer. Complex thermoelectric materials. In *materials for sustainable energy: a collection of peer-reviewed research and review articles from Nature Publishing Group*, pages 101–110. World Scientific, 2011.

[109] C. Gayner and K. K. Kar. Recent advances in thermoelectric materials. *Progress in Materials Science*, 83:330–382, 2016.

[110] J. He and T. M. Tritt. Advances in thermoelectric materials research: Looking back and moving forward. *Science*, 357(6358):eaak9997, 2017.

[111] T. M. Tritt, H. Böttner, and L. Chen. Thermoelectrics: Direct solar thermal energy conversion. *MRS bulletin*, 33(4):366–368, 2008.

[112] L. D. Hicks and M. S. Dresselhaus. Thermoelectric figure of merit of a one-dimensional conductor. *Physical Review B*, 47(24):16631, 1993.

[113] L. D. Hicks and M. S. Dresselhaus. Effect of quantum-well structures on the thermoelectric figure of merit. *Physical Review B*, 47(19):12727, 1993.

[114] D. Li, Y. Wu, P. Kim, L. Shi, P. Yang, and A. Majumdar. Thermal conductivity of individual silicon nanowires. *Applied Physics Letters*, 83(14):2934–2936, 2003.

[115] A. I. Hochbaum, R. Chen, R. D. Delgado, W. Liang, E. C. Garnett, M. Najarian, A. Majumdar, and P. Yang. Enhanced thermoelectric performance of rough silicon nanowires. *Nature*, 451(7175):163–167, 2008.

[116] A. I. Boukai, Y. Bunimovich, J. Tahir-Kheli, J.-K. Yu, W. A. Goddard Iii, and J. R. Heath. Silicon nanowires as efficient thermoelectric materials. *Nature*, 451(7175):168–171, 2008.

[117] B. Kubala, J. König, and J. Pekola. Violation of the wiedemann-franz law in a single-electron transistor. *Physical Review Letters*, 100(6):066801, 2008.

[118] B. Dutta, J. T. Peltonen, D. S. Antonenko, M. Meschke, M. A. Skvortsov, B. Kubala, J. König, C. B. Winkelmann, H. Courtois, and J. P. Pekola. Thermal conductance of a single-electron transistor. *Physical Review Letters*, 119(7):077701, 2017.

[119] R. S. Whitney. Most efficient quantum thermoelectric at finite power output. *Physical Review Letters*, 112(13):130601, 2014.

[120] H. Karbaschi, J. Lovén, K. Courteaut, A. Wacker, and M. Leijnse. Nonlinear thermoelectric efficiency of superlattice-structured nanowires. *Physical Review B*, 94:115414, Sep 2016.

[121] P. Priyadarshi, A. Sharma, S. Mukherjee, and B. Muralidharan. Superlattice design for optimal thermoelectric generator performance. *Journal of Physics D: Applied Physics*, 51(18):185301, 2018.

[122] C. H. Schiegg, M. Dzierzawa, and U. Eckern. Implementation of transmission functions for an optimized three-terminal quantum dot heat engine. *Journal of Physics: Condensed Matter*, 29(8):085303, 2017.

[123] P. Samuelsson, S. Kheradsoud, and B. Sothmann. Optimal quantum interference thermoelectric heat engine with edge states. *Physical Review Letters*, 118(25):256801, 2017.

[124] G. Haack and F. Giazotto. Efficient and tunable aharonov-bohm quantum heat engine. *Physical Review B*, 100(23):235442, 2019.

[125] G. D. Mahan and J. O. Sofo. The best thermoelectric. *Proceedings of the National Academy of Sciences*, 93(15):7436–7439, 1996.

[126] P. Murphy, S. Mukerjee, and J. Moore. Optimal thermoelectric figure of merit of a molecular junction. *Physical Review B*, 78(16):161406, 2008.

[127] C. Van den Broeck. Carnot efficiency revisited. *Advances in Chemical Physics*, 135:189, 2007.

[128] N. Nakpathomkun, H. Q. Xu, and H. Linke. Thermoelectric efficiency at maximum power in low-dimensional systems. *Physical Review B*, 82(23):235428, 2010.

[129] D. M. Kennes, D. Schuricht, and V. Meden. Efficiency and power of a thermoelectric quantum dot device. *EPL (Europhysics Letters)*, 102(5):57003, 2013.

[130] M. A. Sierra and D. Sánchez. Strongly nonlinear thermovoltage and heat dissipation in interacting quantum dots. *Physical Review B*, 90(11):115313, 2014.

[131] A. Svilans, A. M. Burke, S. F. Svensson, M. Leijnse, and H. Linke. Nonlinear thermoelectric response due to energy-dependent transport properties of a quantum dot. *Physica E: Low-dimensional Systems and Nanostructures*, 82:34–38, 2016.

[132] S. Limpert, S. Bremner, and H. Linke. Reversible electron–hole separation in a hot carrier solar cell. *New Journal of Physics*, 17(9):095004, 2015.

[133] A. A. M. Staring, L. W. Molenkamp, B. W. Alphenaar, H. Van Houten, O. J. A. Buyk, M. A. A. Mabesoone, C. W. J. Beenakker, and C. T. Foxon. Coulomb-blockade oscillations in the thermopower of a quantum dot. *EPL (Europhysics Letters)*, 22(1):57, 1993.

[134] A. S. Dzurak, C. G. Smith, M. Pepper, D. A. Ritchie, J. E. F. Frost, G. A. C. Jones, and D. G. Hasko. Observation of coulomb blockade oscillations in the thermopower of a quantum dot. *Solid state communications*, 87(12):1145–1149, 1993.

[135] R. Scheibner, E. G. Novik, T. Borzenko, M. König, D. Reuter, A. Wieck, H. Buhmann, and L. W. Molenkamp. Sequential and cotunneling behavior in the temperature-dependent thermopower of few-electron quantum dots. *Physical Review B*, 75(4):041301, 2007.

[136] S. F. Svensson, A. I. Persson, E. A. Hoffmann, N. Nakpathomkun, H. A. Nilsson, H. Q. Xu, L. Samuelson, and H. Linke. Lineshape of the thermopower of quantum dots. *New Journal of Physics*, 14(3):033041, 2012.

[137] S. F. Svensson, E. A. Hoffmann, N. Nakpathomkun, P. M. Wu, H. Q. Xu, H. A. Nilsson, D. Sánchez, V. Kashcheyevs, and H. Linke. Nonlinear thermovoltage and thermocurrent in quantum dots. *New Journal of Physics*, 15(10):105011, 2013.

[138] M. Turek and K. A. Matveev. Cotunneling thermopower of single electron transistors. *Physical Review B*, 65(11):115332, 2002.

[139] J. Koch, F. von Oppen, Y. Oreg, and E. Sela. Thermopower of single-molecule devices. *Physical Review B*, 70(19):195107, 2004.

[140] A. Svilans, M. Leijnse, and H. Linke. Experiments on the thermoelectric properties of quantum dots. *Comptes Rendus Physique*, 17(10):1096–1108, 2016.

[141] P. A. Erdman, J. T. Peltonen, B. Bhandari, B. Dutta, H. Courtois, R. Fazio, F. Taddei, and J. P. Pekola. Nonlinear thermovoltage in a single-electron transistor. *Physical Review B*, 99(16):165405, 2019.

[142] N. Walldorf, A.-P. Jauho, and K. Kaasbjerg. Thermoelectrics in coulomb-coupled quantum dots: Cotunneling and energy-dependent lead couplings. *Physical Review B*, 96(11):115415, 2017.

[143] A.-M. Daré and P. Lombardo. Powerful coulomb-drag thermoelectric engine. *Physical Review B*, 96(11):115414, 2017.

[144] B. Sothmann, R. Sánchez, and A. N. Jordan. Thermoelectric energy harvesting with quantum dots. *Nanotechnology*, 26(3):032001, 2014.

[145] R. Sánchez and M. Büttiker. Optimal energy quanta to current conversion. *Physical Review B*, 83(8):085428, 2011.

[146] B. Sothmann, R. Sánchez, A. N. Jordan, and M. Büttiker. Rectification of thermal fluctuations in a chaotic cavity heat engine. *Physical Review B*, 85(20):205301, 2012.

[147] R. Sánchez, H. Thierschmann, and L. W. Molenkamp. Single-electron thermal devices coupled to a mesoscopic gate. *New Journal of Physics*, 19(11):113040, 2017.

[148] A.-M. Daré. Comparative study of heat-driven and power-driven refrigerators with coulomb-coupled quantum dots. *Physical Review B*, 100(19):195427, 2019.

[149] R. Sánchez, B. Sothmann, A. N. Jordan, and M. Büttiker. Correlations of heat and charge currents in quantum-dot thermoelectric engines. *New Journal of Physics*, 15(12):125001, 2013.

[150] Y. Zhang, G. Lin, and J. Chen. Three-terminal quantum-dot refrigerators. *Physical Review E*, 91(5):052118, 2015.

[151] R. S. Whitney, R. Sánchez, F. Haupt, and J. Splettstoesser. Thermoelectricity without absorbing energy from the heat sources. *Physica E: Low-dimensional Systems and Nanostructures*, 75:257–265, 2016.

[152] R. S. Whitney. Quantum coherent three-terminal thermoelectrics: maximum efficiency at given power output. *Entropy*, 18(6):208, 2016.

[153] H. L. Edwards, Q. Niu, and A. L. De Lozanne. A quantum-dot refrigerator. *Applied physics letters*, 63(13):1815–1817, 1993.

[154] B. Sothmann, R. Sánchez, A. N. Jordan, and M. Büttiker. Powerful energy harvester based on resonant-tunneling quantum wells. *New Journal of Physics*, 15(9):095021, 2013.

[155] A. N. Jordan, B. Sothmann, R. Sánchez, and M. Büttiker. Powerful and efficient energy harvester with resonant-tunneling quantum dots. *Physical Review B*, 87(7):075312, 2013.

[156] H. Thierschmann, R. Sánchez, B. Sothmann, F. Arnold, C. Heyn, W. Hansen, H. Buhmann, and L. W. Molenkamp. Three-terminal energy harvester with coupled quantum dots. *Nature nanotechnology*, 10(10):854–858, 2015.

[157] G. Jaliel, R. K. Puddy, R. Sánchez, A. N. Jordan, B. Sothmann, I. Farrer, J. P. Griffiths, D. A. Ritchie, and C. G. Smith. Experimental realization of a quantum dot energy harvester. *Physical Review Letters*, 123(11):117701, 2019.

[158] J. P. Small, K. M. Perez, and P. Kim. Modulation of thermoelectric power of individual carbon nanotubes. *Physical Review Letters*, 91(25):256801, 2003.

[159] M. C. Llaguno, J. E. Fischer, A. T. Johnson, and J. Hone. Observation of thermopower oscillations in the coulomb blockade regime in a semiconducting carbon nanotube. *Nano Letters*, 4(1):45–49, 2004.

[160] A. G. Pogosov, M. V. Budantsev, R. A. Lavrov, A. E. Plotnikov, A. K. Bakarov, A. I. Toropov, and J. C. Portal. Coulomb blockade and the thermopower of a suspended quantum dot. *JETP letters*, 83(3):122–126, 2006.

[161] S. Jezouin, F. D. Parmentier, A. Anthore, U. Gennser, A. Cavanna, Y. Jin, and F. Pierre. Quantum limit of heat flow across a single electronic channel. *Science*, 342(6158):601–604, 2013.

[162] L. Cui, W. Jeong, S. Hur, M. Matt, J. C. Klöckner, F. Pauly, P. Nielaba, J. C. Cuevas, E. Meyhofer, and P. Reddy. Quantized thermal transport in single-atom junctions. *Science*, 355(6330):1192–1195, 2017.

[163] E. Sivre, A. Anthore, F. D. Parmentier, A. Cavanna, U. Gennser, A. Ouerghi, Y. Jin, and F. Pierre. Heat coulomb blockade of one ballistic channel. *Nature Physics*, 14(2):145–148, 2018.

[164] B. Dutta, D. Majidi, N. W. Talarico, N. L. Gullo, C. B. Winkelmann, and H. Courtois. A single-quantum-dot heat valve. *arXiv preprint arXiv:2001.08183*, 2020.

[165] D. Prete, P. A. Erdman, V. Demontis, V. Zannier, D. Ercolani, L. Sorba, F. Beltram, F. Rossella, F. Taddei, and S. Roddaro. Thermoelectric conversion at 30 k in inas/inp nanowire quantum dots. *Nano Letters*, 19(5):3033–3039, 2019.

[166] E. A. Hoffmann, N. Nakpathomkun, A. I. Persson, H. Linke, H. A. Nilsson, and L. Samuelson. Quantum-dot thermometry. *Applied Physics Letters*, 91(25):252114, 2007.

[167] A. V. Feshchenko, L. Casparis, I. M. Khaymovich, D. Maradan, O.-P. Saira, M. Palma, M. Meschke, J. P. Pekola, and D. Zumbühl. Tunnel-junction thermometry down to millikelvin temperatures. *Physical Review Applied*, 4(3):034001, 2015.

[168] D. Mandal and C. Jarzynski. Work and information processing in a solvable model of maxwell's demon. *Proceedings of the National Academy of Sciences*, 109(29):11641–11645, 2012.

[169] Z. Lu, D. Mandal, and C. Jarzynski. Engineering maxwell's demon. *Physics Today*, 67(8):60–61, 2014.

[170] A. Bérut, A. Arakelyan, A. Petrosyan, S. Ciliberto, R. Dillenschneider, and E. Lutz. Experimental verification of landauer's principle linking information and thermodynamics. *Nature*, 483(7388):187–189, 2012.

[171] Y. Jun, M. Gavrilov, and J. Bechhoefer. High-precision test of landauer's principle in a feedback trap. *Physical Review Letters*, 113(19):190601, 2014.

[172] J. V. Koski, V. F. Maisi, J. P. Pekola, and D. V. Averin. Experimental realization of a szilard engine with a single electron. *Proceedings of the National Academy of Sciences*, 111(38):13786–13789, 2014.

[173] J. Hong, B. Lambson, S. Dhuey, and J. Bokor. Experimental test of landauer's principle in single-bit operations on nanomagnetic memory bits. *Science advances*, 2(3):e1501492, 2016.

[174] M. Gavrilov. Erasure without work in an asymmetric, double-well potential. In *Experiments on the Thermodynamics of Information Processing*, pages 83–96. Springer, 2017.

[175] M. Ribezzi-Crivellari and F. Ritort. Large work extraction and the landauer limit in a continuous maxwell demon. *Nature Physics*, 15(7):660–664, 2019.

[176] J. A. Vaccaro and S. M. Barnett. Information erasure without an energy cost. *Proceedings of the Royal Society A: Mathematical, Physical and Engineering Sciences*, 467(2130):1770–1778, 2011.

[177] S. M. Barnett and J. A. Vaccaro. Beyond landauer erasure. *Entropy*, 15(11):4956–4968, 2013.

[178] J. V. Koski, V. F. Maisi, T. Sagawa, and J. P. Pekola. Experimental observation of the role of mutual information in the nonequilibrium dynamics of a maxwell demon. *Physical Review Letters*, 113(3):030601, 2014.

[179] J. V. Koski, A. Kutvonen, I. M. Khaymovich, T. Ala-Nissila, and J. P. Pekola. On-chip maxwell's demon as an information-powered refrigerator. *Physical Review Letters*, 115(26):260602, 2015.

[180] K. Chida, S. Desai, K. Nishiguchi, and A. Fujiwara. Power generator driven by maxwell's demon. *Nature communications*, 8(1):1–7, 2017.

[181] N. Cottet, S. Jezouin, L. Bretheau, P. Campagne-Ibarcq, Q. Ficheux, J. Anders, A. Auffèves, R. Azouit, P. Rouchon, and B. Huard. Observing a quantum maxwell demon at work. *Proceedings of the National Academy of Sciences*, 114(29):7561–7564, 2017.

[182] M. Naghiloo, J. J. Alonso, A. Romito, E. Lutz, and K. W. Murch. Information gain and loss for a quantum maxwell's demon. *Physical Review Letters*, 121(3):030604, 2018.

[183] Y. Masuyama, K. Funo, Y. Murashita, A. Noguchi, S. Kono, Y. Tabuchi, R. Yamazaki, M. Ueda, and Y. Nakamura. Information-to-work conversion by maxwell's demon in a superconducting circuit quantum electrodynamical system. *Nature communications*, 9(1):1–6, 2018.

[184] S. Vinjanampathy and J. Anders. Quantum thermodynamics. *Contemporary Physics*, 57(4):545–579, 2016.

[185] F. Binder, L. A. Correa, C. Gogolin, J. Anders, and G. Adesso. Thermodynamics in the quantum regime. *Fundamental Theories of Physics (Springer, 2018)*, 2018.

[186] R. Alicki. The quantum open system as a model of the heat engine. *Journal of Physics A: Mathematical and General*, 12(5):L103, 1979.

[187] M. O. Scully, M. S. Zubairy, G. S. Agarwal, and H. Walther. Extracting work from a single heat bath via vanishing quantum coherence. *Science*, 299(5608):862–864, 2003.

[188] R. Dillenschneider and E. Lutz. Energetics of quantum correlations. *EPL (Europhysics Letters)*, 88(5):50003, 2009.

[189] N. Brunner, M. Huber, N. Linden, S. Popescu, R. Silva, and P. Skrzypczyk. Entanglement enhances cooling in microscopic quantum refrigerators. *Physical Review E*, 89(3):032115, 2014.

[190] P. Kammerlander and J. Anders. Coherence and measurement in quantum thermodynamics. *Scientific reports*, 6(1):1–7, 2016.

[191] J. B. Brask, G. Haack, N. Brunner, and M. Huber. Autonomous quantum thermal machine for generating steady-state entanglement. *New Journal of Physics*, 17(11):113029, 2015.

[192] L. L. Yan, T. P. Xiong, K. Rehan, F. Zhou, D. F. Liang, L. Chen, J. Q. Zhang, W. L. Yang, Z. H. Ma, and M. Feng. Single-atom demonstration of the quantum landauer principle. *Physical Review Letters*, 120:210601, 2018.

[193] R. Gaudenzi, E. Burzurí, S. Maegawa, H. S. J. van der Zant, and F. Luis. Quantum landauer erasure with a molecular nanomagnet. *Nature Physics*, 14(6):565–568, 2018.

[194] J. R. Petta, A. C. Johnson, J. M. Taylor, E. A. Laird, A. Yacoby, M. D. Lukin, C. M. Marcus, M. P. Hanson, and A. C. Gossard. Coherent manipulation of coupled electron spins in semiconductor quantum dots. *Science*, 309(5744):2180–2184, 2005.

[195] R. Miao, H. Xu, M. Skripnik, L. Cui, K. Wang, K. G. Pedersen, M. Leijnse, F. Pauly, K. Warnmark, E. Meyhofer, et al. Influence of quantum interference on the thermoelectric properties of molecular junctions. *Nano letters*, 18(9):5666–5672, 2018.

Acknowledgments

I have had the privilege to be surrounded by many brilliant and inspiring people during my work and studies that preceded this thesis. Several of those people have contributed significantly, directly and indirectly, to my work and academic life, both as scientists and as friends. I will here take the opportunity to thank them.

Most importantly, I would like to express my deep gratitude to my advisor Martin. I have always appreciated your support and trust when I delve into what I find interesting at the moment. This have given me a much appreciated feeling of freedom and independence, while I've always felt I could come to you for support and guidance when I needed it. That, together with our shared sense of what is interesting science, and how it's conducted, have made the last five years very enjoyable.

I would also like to say thank you to Artis, Adam, Heiner and Sven. In addition to countless interesting discussions it's been a privilege to be surrounded by your world-class experiments, and I am grateful for the successful collaborations we have had during the work discussed in this thesis, and beyond.

A special thanks goes to current and former long-time members of the Leijnse group: Florinda, Michael, Thanos, Ruben, Zeng-Zhao and Simon. I've appreciated our interactions a lot since one can feel pretty isolated as a theorist surrounded by experimentalists. Besides, you are all interesting people contributing to a pleasant working environment.

Speaking of the working environment, a few friends have made FTF an especially good place to work. Thank you Calle, Marcus, Mårten, Laura and Abdul-Rehman for all the fun times we've had at work. An honorable mention also goes out to the members of Dr. Nano.

Finally, I would like to thank my family and friends for their support and for making life outside the university very enjoyable. Because, believe it or not, there is more to life than physics.